


QGSJET-III model of high energy hadronic interactions: The formalism

Sergey Ostapchenko

Universität Hamburg, II Institut für Theoretische Physik, 22761 Hamburg, Germany (Received 24 November 2023; accepted 10 January 2024; published 5 February 2024)

The physics content of the QGSJET-III Monte Carlo generator of high energy hadronic collisions is described. In particular, a phenomenological implementation of higher twist corrections to hard parton scattering processes is discussed in some detail. Additionally addressed is the treatment of the so-called “color fluctuation” effects related to a decomposition of hadron wave functions into a number of Fock states characterized by different spatial sizes and different parton densities. Selected model results regarding the energy dependence of the total, elastic, and diffractive proton-proton cross sections are presented.

DOI: [10.1103/PhysRevD.109.034002](https://doi.org/10.1103/PhysRevD.109.034002)**I. INTRODUCTION**

Nowadays high energy experiments both in the collider and cosmic ray (CR) fields imply an extensive use of Monte Carlo (MC) generators of hadronic interactions. At colliders, the primary goal of such generators is to describe Standard Model backgrounds for new physics searches and to confront novel theoretical ideas to experimental data. On the other hand, in the CR field, MC models of high energy interactions play an important role, when interpreting experimental data. This is particularly so for investigations of very high energy CRs, which are performed by indirect methods: studying various characteristics of extensive air showers (EAS)—huge nuclear-electromagnetic cascades induced by interactions of primary CR particles in the atmosphere of the Earth—and reconstructing the properties of those particles, based on the measured EAS characteristics. Such applications imply a number of requirements to CR interaction models. Those should be able to provide a reasonable description of collisions with nuclei of various hadron species, primarily, of (anti)nucleons, pions, and kaons, over a wide energy range: from fixed target energies up to some 10^{12} GeV laboratory energy. Additionally, the steeply falling down primary CR flux and the cascade nature of extensive air showers enhance the importance of forward secondary particle production. Last but not least, given the scarcity of available experimental data regarding such forward production and the lack of possibility to retune MC generators, based on CR data, a substantial predictive power is required from CR interaction models.

Over the past three decades, the QGSJET [1–3] and QGSJET-II [4–6] MC generators proved to be very successful regarding the analyses and interpretations of various CR data, notably, from air shower experiments. In the current work, we report a further development of the model framework, related to taking into consideration the so-called dynamical higher twist corrections to hard parton scattering processes and to the implementation of “color fluctuation” effects in high energy hadronic collisions. While the treatment of secondary particle production and the application of the model to calculations of EAS characteristics will be discussed elsewhere [7], we concentrate here on the description of the model formalism, providing also some selected results regarding the energy dependence of the total, elastic, and diffractive proton-proton cross sections.

The paper is organized as follows. In Sec. II, we discuss the Reggeon field theory (RFT) approach to multiple scattering in hadronic collisions. Section III is devoted to the treatment of hard parton scattering within the RFT framework. In Sec. IV, we address the implementation of color fluctuation effects. The treatment of nonlinear interaction effects due to Pomeron-Pomeron interactions is described in Sec. V. Section VI is devoted to phenomenological implementation of dynamical power corrections to hard parton scattering. The model generalization to the case of nuclear collisions and the MC realization of the formalism are described in Sec. VII. In Sec. VIII, we present and discuss selected model results. Finally, we conclude in Sec. IX.

II. MULTIPLE SCATTERING IN THE REGGEON FIELD THEORY

High energy hadronic collisions are predominantly multiple scattering processes, being mediated by multiple parton cascades developing between the interacting

Published by the American Physical Society under the terms of the Creative Commons Attribution 4.0 International license. Further distribution of this work must maintain attribution to the author(s) and the published article's title, journal citation, and DOI. Funded by SCOAP³.

projectile and target hadrons (nuclei). While a perturbative description of multiple scattering (so-called multiparton interactions) is an actively developing field (see, e.g., [8] for a review), the corresponding treatment in MC generators has to rely presently on the old RFT formalism [9].

Since the underlying, so to say “elementary,” parton cascades develop, at least partly, in the nonperturbative domain of low parton virtualities, where the notion of partons can be used for a qualitative discussion only, one is forced to rely on an effective macroscopic description for such cascades—treating them as Pomeron exchanges. The Pomeron exchange eikonal (the imaginary part¹ of the corresponding amplitude) is usually chosen in the form

$$\chi_{hp}^{\mathbb{P}}(s, b) = \frac{\gamma_h \gamma_p (s/s_0)^{\alpha_{\mathbb{P}}(0)-1}}{R_h^2 + R_p^2 + \alpha'_{\mathbb{P}}(0) \ln(s/s_0)} \times \exp \left[-\frac{b^2/4}{R_h^2 + R_p^2 + \alpha'_{\mathbb{P}}(0) \ln(s/s_0)} \right], \quad (1)$$

where $\alpha_{\mathbb{P}}(0)$ and $\alpha'_{\mathbb{P}}(0)$ are, respectively, the intercept and the slope of the Pomeron Regge trajectory, γ_h is the residue and R_h^2 the slope for the Pomeron coupling to hadron h , s and b are, correspondingly, the center-of-mass (c.m.) energy squared and impact parameter for the collision, and $s_0 \simeq 1 \text{ GeV}^2$ —the hadronic mass scale.

Using the eikonal description for multiple Pomeron emission vertices, one obtains the well-known simple expressions for the total and elastic hadron-proton cross sections:

$$\sigma_{hp}^{\text{tot}}(s) = 2 \int d^2b \left[1 - e^{-\chi_{hp}^{\mathbb{P}}(s,b)} \right] \quad (2)$$

$$\sigma_{pp}^{\text{el}}(s) = \int d^2b \left[1 - e^{-\chi_{hp}^{\mathbb{P}}(s,b)} \right]^2. \quad (3)$$

Moreover, considering unitarity cuts of the corresponding elastic scattering diagrams shown schematically in Fig. 1 and applying the so-called Abramovskii-Gribov-Kancheli (AGK) cutting rules [10], one is able to obtain partial cross sections for various inelastic final states corresponding to having precisely n “elementary” production processes (n cut Pomerons):

$$\sigma_{hp}^{(n)}(s) = \int d^2b \frac{\left[2\chi_{hp}^{\mathbb{P}}(s, b) \right]^n}{n!} e^{-2\chi_{hp}^{\mathbb{P}}(s,b)}. \quad (4)$$

To describe secondary particle production, one assumes that each cut Pomeron corresponds to a creation of a pair of strings of color field, stretched between constituent partons

¹The real part of the Pomeron amplitude can be neglected in the high energy limit.

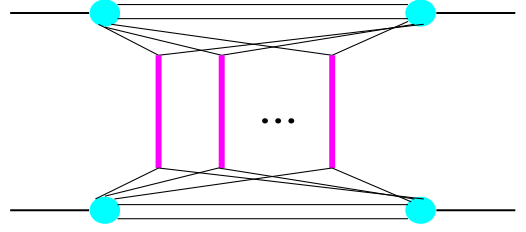


FIG. 1. General multi-Pomeron contribution to hadron-hadron scattering amplitude; elementary scattering processes (vertical thick lines) are described as Pomeron exchanges.

[(anti)quarks or (anti)diquarks] of the interacting hadrons and models the breakup of those strings by means of suitable string fragmentation procedures [11,12]. Importantly, the corresponding parameters can be expressed via intercepts of secondary Regge trajectories [13].

III. TREATING HARD SCATTERING WITHIN THE RFT FRAMEWORK

While the original Gribov’s formulation of RFT relied on the assumption that the bulk of hadron production is characterized by small transverse momenta [9], $p_t \lesssim 1 \text{ GeV}$, the contribution of the so-called semihard processes corresponding to parton cascades developing, at least partly, in the high p_t domain becomes increasingly important in the very high energy limit. Indeed, the smallness of the corresponding strong coupling, $\alpha_s(p_t^2)$, in such cascades becomes compensated by large collinear and infrared logarithms and by a high parton density [14]. To treat such processes within the RFT framework, the so-called “semihard Pomeron” approach has been proposed [2,15–17] (see also [18] for a recent discussion). The underlying basic idea was to employ the above-discussed phenomenological Pomeron description for purely “soft” nonperturbative (parts of) parton cascades: for parton virtualities $|q^2| < Q_0^2$, while treating parton evolution in the perturbative $|q^2| > Q_0^2$ domain by means of the Dokshitzer-Gribov-Lipatov-Altarelli-Parisi (DGLAP) formalism [19–21], with Q_0^2 being some chosen virtuality cutoff for the perturbative quantum chromodynamics (pQCD) to be applicable. This allowed one to develop a Pomeron calculus, based on a “general Pomeron,” the latter being a sum of the soft and semihard ones, as shown symbolically in Fig. 2.

In particular, Eqs. (2)–(4) hold upon defining the eikonal $\chi_{hp}^{\mathbb{P}}$ as a sum $\chi_{hp}^{\mathbb{P}\text{soft}} + \chi_{hp}^{\mathbb{P}\text{sh}}$, where $\chi_{hp}^{\mathbb{P}\text{soft}}$ is given by Eq. (1), while for $\chi_{hp}^{\mathbb{P}\text{sh}}$ one obtains [16,17]

$$\begin{aligned} \chi_{hp}^{\mathbb{P}\text{sh}}(s, b) &= \frac{1}{2} \sum_{I,J} \int d^2b' \int \frac{dx^+ dx^-}{x^+ x^-} \\ &\times \chi_{Ih}^{\mathbb{P}\text{soft}} \left(\frac{s_0}{x^+}, b' \right) \chi_{Jp}^{\mathbb{P}\text{soft}} \left(\frac{s_0}{x^-}, |\vec{b} - \vec{b}'| \right) \\ &\times \sigma_{IJ}^{\text{QCD}}(x^+ x^- s, Q_0^2, Q_0^2). \end{aligned} \quad (5)$$

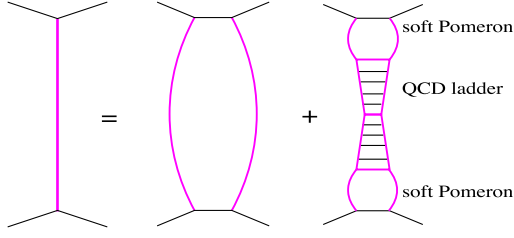


FIG. 2. A general Pomeron (left-hand side) consists of the soft and semihard ones—correspondingly the first and the second contributions in the right-hand side.

Here $\sigma_{IJ}^{\text{QCD}}(\hat{s}, q_1^2, q_2^2)$ corresponds to the contribution of the DGLAP parton “ladder,” with the ladder leg partons I and J [(anti)quarks or gluons²] characterized by the virtualities q_1^2 and q_2^2 , respectively:

$$\begin{aligned} \sigma_{IJ}^{\text{QCD}}(\hat{s}, q_1^2, q_2^2) &= K \sum_{I', J'} \int dz^+ dz^- \int dp_t^2 \\ &\times E_{I'I'}^{\text{QCD}}(z^+, q_1^2, \mu_F^2) E_{J'J}^{\text{QCD}}(z^-, q_2^2, \mu_F^2) \\ &\times \frac{d\sigma_{I'J'}^{2 \rightarrow 2}(z^+ z^- \hat{s}, p_t^2, \mu_R)}{dp_t^2} \\ &\times \Theta(\mu_F^2 - \max[q_1^2, q_2^2]), \end{aligned} \quad (6)$$

where $d\sigma_{IJ}^{2 \rightarrow 2}/dp_t^2$ is the Born parton cross section, p_t being the parton transverse momentum in the hard process, μ_F and μ_R are the factorization and renormalization scales, respectively (we use $\mu_F = \mu_R = p_t/2$), and the factor $K = 1.5$ takes effectively into account higher order QCD corrections. $E_{I'I'}^{\text{QCD}}(z, q^2, \mu_F^2)$ describes parton density evolution from the scale q^2 to μ_F^2 , subject to the initial condition $E_{I'I'}^{\text{QCD}}(z, q^2, q^2) = \delta_I^I \delta(1-z)$.

In turn, the eikonal χ_{Ih}^{Psoft} corresponding to a soft Pomeron exchange between hadron h and parton I is obtained from Eq. (1), neglecting the small slope of the Pomeron-parton coupling $R_I^2 \sim 1/Q_0^2$ and replacing the vertex γ_p by a parametrized Pomeron-parton vertex $V_{I/h}^{\text{P}}$:

$$\begin{aligned} \chi_{Ih}^{\text{Psoft}}(\hat{s}, b) &= \frac{\gamma_h V_{I/h}^{\text{P}}(s_0/\hat{s})(\hat{s}/s_0)^{\alpha_{\text{P}}(0)-1}}{R_h^2 + \alpha_{\text{P}}'(0) \ln(\hat{s}/s_0)} \\ &\times \exp\left[-\frac{b^2/4}{R_h^2 + \alpha_{\text{P}}'(0) \ln(\hat{s}/s_0)}\right]. \end{aligned} \quad (7)$$

We use³ [17]

²We shall not discuss explicitly the contribution of hard interactions of valence quarks; see, e.g., [16] for the corresponding details.

³The ansatz, Eqs. (8) and (9), differs from the one used in [16,17] by the factor $(1+x)^{b_h}$ chosen to improve the large x behavior of gluon PDFs. More sophisticated parametrizations may generally be used for $V_{I/h}^{\text{P}}$.

$$V_{g/h}^{\text{P}}(x) = r_{g/\text{P}}(1-w_{qg})(1-x)^{\beta_{g/h}} \times (1+x)^{b_h} \quad (8)$$

$$\begin{aligned} V_{q/h}^{\text{P}}(x) &= r_{g/\text{P}} w_{qg} \int_x^1 dz z^{\alpha_{\text{P}}(0)-1} \\ &\times P_{qg}(z)(1-x/z)^{\beta_{g/h}}(1+x/z)^{b_h}, \end{aligned} \quad (9)$$

where P_{qg} is the usual Altarelli-Parisi splitting kernel for three active flavors and the parameter $r_{g/\text{P}}$ characterizes gluon density in the soft Pomeron in the low x limit, when probed at the virtuality scale Q_0^2 . We use $\beta_{g/p} = 4$ and $\beta_{g/\pi} = \beta_{g/K} = 2$, while the constants b_h are fixed requiring momentum conservation for parton distribution functions (PDFs).

By construction, the eikonal χ_{Ih}^{Psoft} is related to the generalized parton distribution (GPD) $G_{I/h}$ at the virtuality scale Q_0^2 [4,22]:

$$xG_{I/h}(x, b, Q_0^2) = \chi_{Ih}^{\text{Psoft}}(s_0/x, b). \quad (10)$$

It is further noteworthy that the above-discussed semihard Pomeron approach largely resembles the “heterotic Pomeron” concept proposed in [23] (see also [24]). In particular, the relatively large slope α_{P}' of the soft Pomeron gives rise to a rather fast transverse expansion of parton “clouds.” On the other hand, the perturbative ($|q^2| > Q_0^2$) parton evolution, being characterized by small transverse displacements ($\lesssim 1/Q_0$), leads to a quick rise of parton density.

IV. TREATMENT OF COLOR FLUCTUATIONS

One of the drawbacks of the scheme discussed so far is that it offers no room for inelastic diffraction. To overcome that, one has to account for transitions of interacting hadrons into various excited states, after each elementary rescattering process (Pomeron exchange) [25]. This can be conveniently done following the Good-Walker (GW) approach [26] (see, e.g., [27] for a recent discussion): assuming both the original hadron h and its excited states h^* to be represented by a superposition of eigenstates of the scattering matrix:

$$|h\rangle = \sum_i \sqrt{C_h^{(i)}} |i\rangle \quad (11)$$

$$|h^*\rangle = \sum_i \sqrt{C_{h^*}^{(i)}} |i\rangle, \quad (12)$$

with $C_h^{(i)}$, $C_{h^*}^{(i)}$ being the corresponding partial weights ($\sum_i C_h^{(i)} = \sum_i C_{h^*}^{(i)} = 1$).

In such an approach, one arrives to a trivial generalization of Eqs. (2)–(4), averaging over different combinations of GW Fock states:

$$\sigma_{hp}^{\text{tot}}(s) = 2 \int d^2b \sum_{i,j} C_h^{(i)} C_p^{(j)} \left[1 - e^{-\chi_{hp(ij)}^{\text{P}}(s,b)} \right] \quad (13)$$

$$\sigma_{hp}^{\text{el}}(s) = \int d^2b \left[\sum_{i,j} C_h^{(i)} C_p^{(j)} \left(1 - e^{-\chi_{hp(ij)}^{\text{P}}(s,b)} \right) \right]^2 \quad (14)$$

$$\sigma_{hp}^{(n)}(s) = \int d^2b \sum_{i,j} C_h^{(i)} C_p^{(j)} \times \frac{\left[2\chi_{hp(ij)}^{\text{P}}(s,b) \right]^n}{n!} \exp(-2\chi_{hp(ij)}^{\text{P}}(s,b)). \quad (15)$$

Here the eikonals $\chi_{hp(ij)}^{\text{P}} = \chi_{hp(ij)}^{\text{soft}} + \chi_{hp(ij)}^{\text{sh}}$ correspond to exchanges of both soft and semihard Pomerons between GW states $|i\rangle$ and $|j\rangle$ of the projectile and the target, respectively.

In turn, the inelastic cross section is now split into the ‘‘absorptive’’ and diffractive parts:

$$\sigma_{hp}^{\text{inel}}(s) \equiv \sigma_{hp}^{\text{tot}}(s) - \sigma_{hp}^{\text{el}}(s) = \sigma_{hp}^{\text{abs}}(s) + \sigma_{hp}^{\text{diffr}}(s), \quad (16)$$

with the former corresponding to any number ($n \geq 1$) of cut Pomeron exchanges,

$$\begin{aligned} \sigma_{hp}^{\text{abs}}(s) &= \sum_{n=1}^{\infty} \sigma_{hp}^{(n)}(s) \\ &= \int d^2b \sum_{i,j} C_h^{(i)} C_p^{(j)} \left[1 - e^{-2\chi_{hp(ij)}^{\text{P}}(s,b)} \right], \end{aligned} \quad (17)$$

and the latter containing contributions of the projectile, target, and double diffraction.⁴

The corresponding soft Pomeron exchange eikonal is defined as

$$\begin{aligned} \chi_{hp(ij)}^{\text{soft}}(s,b) &= \frac{\gamma_{h(i)} \gamma_{p(j)} (s/s_0)^{\alpha_{\text{P}}(0)-1}}{R_{h(i)}^2 + R_{p(j)}^2 + \alpha'_{\text{P}}(0) \ln(s/s_0)} \\ &\times \exp \left[-\frac{b^2/4}{R_{h(i)}^2 + R_{p(j)}^2 + \alpha'_{\text{P}}(0) \ln(s/s_0)} \right], \end{aligned} \quad (18)$$

taking into consideration that different GW Fock states are generally characterized by different sizes and different couplings to the Pomeron. Moreover, it is quite reasonable to assume that the coupling $\gamma_{h(i)}$ is approximately proportional to the transverse area of the state [11]:

$$\gamma_{h(i)} = g_0 R_{h(i)}^2, \quad (19)$$

using thus a universal parameter g_0 .

The semihard Pomeron eikonal is generalized similarly:

$$\begin{aligned} \chi_{hp(ij)}^{\text{sh}}(s,b) &= \frac{1}{2} \sum_{I,J} \int d^2b' \int \frac{dx^+ dx^-}{x^+ x^-} \\ &\times \chi_{Ih(i)}^{\text{soft}} \left(\frac{s_0}{x^+}, b' \right) \chi_{Jp(j)}^{\text{soft}} \left(\frac{s_0}{x^-}, |\vec{b} - \vec{b}'| \right) \\ &\times \sigma_{IJ}^{\text{QCD}}(x^+ x^- s, Q_0^2, Q_0^2), \end{aligned} \quad (20)$$

where the eikonal $\chi_{Ih(i)}^{\text{soft}}$ corresponds to a soft Pomeron exchange between parton I and GW state $|i\rangle$ of hadron h :

$$\begin{aligned} \chi_{Ih(i)}^{\text{soft}}(\hat{s}, b) &= \frac{\gamma_{h(i)} V_{I/h(i)}^{\text{P}}(s_0/\hat{s}) (\hat{s}/s_0)^{\alpha_{\text{P}}(0)-1}}{R_{h(i)}^2 + \alpha'_{\text{P}}(0) \ln(\hat{s}/s_0)} \\ &\times \exp \left[-\frac{b^2/4}{R_{h(i)}^2 + \alpha'_{\text{P}}(0) \ln(\hat{s}/s_0)} \right], \end{aligned} \quad (21)$$

with $V_{I/h(i)}^{\text{P}}$ being defined by Eqs. (8) and (9), under the replacement $b_h \rightarrow b_{h(i)}$. Here we have an important feature: assuming a universal gluon density $r_{g/\text{P}}$ in the soft Pomeron in the low x limit, at the scale Q_0^2 , the momentum conservation for PDFs for *individual* Fock states,

$$\begin{aligned} x f_{I/h(i)}(x, Q_0^2) &= \int d^2b x G_{I/h(i)}(x, b, Q_0^2) \\ &= \int d^2b \chi_{Ih(i)}^{\text{soft}}(s_0/x, b), \end{aligned} \quad (22)$$

gives rise to different $b_{h(i)}$ for different states. Consequently, partial PDFs $f_{I/h(i)}$ vary considerably from one Fock state to another [28]: with smaller Fock states being characterized by smaller (integrated) parton densities in the low x limit but having harder PDF shapes.

It is noteworthy, however, that the above-discussed approach is applicable, strictly speaking, to the treatment of low mass diffraction only. Indeed, considering hadron h transitions into multiparticle states h^* of arbitrary mass, one can no longer apply the decomposition, Eqs. (11) and (12), based on a finite number of GW states⁵: with increasing energy, larger and larger excited states will play an important role.

In the following, we consider equal probabilities for different GW states, $C_h^{(i)} \equiv 1/N_{\text{GW}}$, using $N_{\text{GW}} = 3$ for any hadron⁶ and choosing a loguniform distribution for $R_{h(i)}^2$:

$$R_{h(i)}^2 = R_{h(1)}^2 d_h^{\frac{i-1}{N_{\text{GW}}-1}}. \quad (23)$$

⁵In principle, one may consider a continuum of intermediate multiparticle states, postulating some energy and mass dependence for the decomposition in Eqs. (11) and (12).

⁶We verified explicitly that using a larger number of GW states does not modify our results significantly.

⁴See, e.g., [5] for the corresponding partial cross sections.

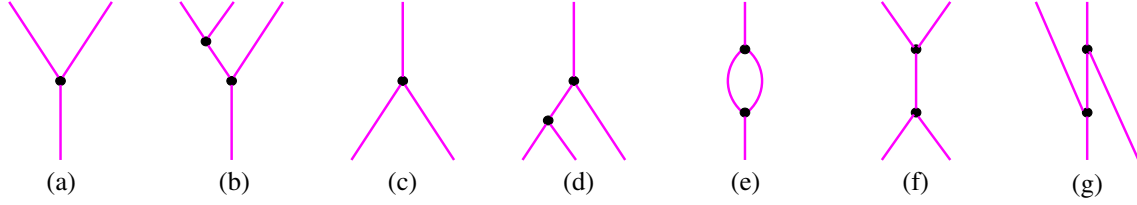


FIG. 3. Simplest examples of enhanced Pomeron diagrams.

V. ENHANCED POMERON DIAGRAMS

The major feature inherited from the previous model version, QGSJET-II [4,5], is a treatment of nonlinear interaction effects, based on all-order resummation of the underlying Pomeron-Pomeron interaction diagrams [29–31]. The simplest examples of such, so-called enhanced, graphs are shown in Fig. 3, which correspond to rescattering of intermediate partons in the elementary parton cascades off the projectile [(a), (b), (f), and (g)] and the target [(c), (d), (f), and (g)] hadrons or off each other [(e)]. Taking such diagrams into consideration amounts to replace the eikonal $\chi_{hp(ij)}^{\mathbb{P}}$ in Eqs. (13)–(15) by $\chi_{hp(ij)}^{\text{scr}} = \chi_{hp(ij)}^{\mathbb{P}} + \chi_{hp(ij)}^{\text{enh}}$, where $\chi_{hp(ij)}^{\text{enh}}$ corresponds to the summary contribution of all significant irreducible enhanced Pomeron graphs exchanged between GW Fock states $|i\rangle$ and $|j\rangle$ of the projectile and the target, respectively.

Using eikonal vertices for the transition of m into n Pomerons ($m + n \geq 3$) [32],

$$G^{(m,n)} = G\gamma_{\mathbb{P}}^{m+n}, \quad (24)$$

with the constant G being related to the triple-Pomeron coupling $r_{3\mathbb{P}}$ as $G = r_{3\mathbb{P}}/(4\pi\gamma_{\mathbb{P}}^3)$, and neglecting the small slope of the triple-Pomeron vertex $R_{3\mathbb{P}}^2$, one was able to obtain $\chi_{hp(ij)}^{\text{enh}}$ in a relatively compact form [5,30,31]:

$$\begin{aligned} \chi_{hp(ij)}^{\text{enh}}(s, b) = & G \int_{\xi}^{Y-\xi} dy' \int d^2b' \\ & \times \left\{ \left[\left(1 - e^{-\chi_{h(i)|p(j)}^{\text{net}}}\right) \left(1 - e^{-\chi_{p(j)|h(i)}^{\text{net}}}\right) \right. \right. \\ & \left. \left. - \chi_{h(i)|p(j)}^{\text{net}} \chi_{p(j)|h(i)}^{\text{net}} \right] - \left[\chi_{h(i)|p(j)}^{\text{net}} - \chi_{h(i)}^{\text{loop}} \right] \right. \\ & \times \left[\left(1 - e^{-\chi_{p(j)|h(i)}^{\text{net}}}\right) e^{-\chi_{h(i)|p(j)}^{\text{net}}} - \chi_{p(j)|h(i)}^{\text{net}} \right] \\ & \left. + \chi_{p(j)}^{\mathbb{P}}(y', b') \left[\chi_{h(i)}^{\text{loop}} - \chi_{h(i)}^{\text{loop}(1)} \right] \right\}. \quad (25) \end{aligned}$$

Here $Y = \ln(s/s_0)$, ξ is the minimal rapidity “size” of the Pomeron, and the omitted arguments of the eikonals read $\chi_{h(i)|p(j)}^{\text{net}} = \chi_{h(i)|p(j)}^{\text{net}}(Y - y', \vec{b} - \vec{b}' | Y, \vec{b})$, $\chi_{p(j)|h(i)}^{\text{net}} = \chi_{p(j)|h(i)}^{\text{net}}(y', \vec{b}' | Y, \vec{b})$, $\chi_{h(i)}^{\text{loop}} = \chi_{h(i)}^{\text{loop}}(Y - y', |\vec{b} - \vec{b}'|)$, $\chi_{h(i)}^{\text{loop}(1)} = \chi_{h(i)}^{\text{loop}(1)}(Y - y', |\vec{b} - \vec{b}'|)$.

The “net-fan” contributions $\chi_{h(i)|p(j)}^{\text{net}}$ are defined by a recursive equation:

$$\begin{aligned} \chi_{h(i)|p(j)}^{\text{net}}(y', \vec{b}' | Y, \vec{b}) = & \chi_{h(i)}^{\text{loop}}(y', b') + G \int d^2b'' \\ & \times \int_{\xi}^{y'-\xi} dy'' \left(1 - e^{-\chi^{\text{loop}}(y'-y'', |\vec{b}' - \vec{b}''|)}\right) \\ & \times \left[\left(1 - e^{-\chi_{h(i)|p(j)}^{\text{net}}(y'', \vec{b}'' | Y, \vec{b})}\right) \right. \\ & \times \exp(-\chi_{p(j)|h(i)}^{\text{net}}(Y - y'', \vec{b} - \vec{b}'' | Y, \vec{b})) \\ & \left. - \chi_{h(i)|p(j)}^{\text{net}}(y'', \vec{b}'' | Y, \vec{b}) \right], \quad (26) \end{aligned}$$

where $\chi_{h(i)}^{\text{loop}}$ and $\chi_{h(i)}^{\text{loop}(1)}$ correspond to general irreducible two-point sequences of Pomerons and Pomeron loops, exchanged between GW state $|i\rangle$ of hadron h and a multi-Pomeron vertex, while χ^{loop} and $\chi^{\text{loop}(1)}$ are contributions of such sequences exchanged between two multi-Pomeron vertices (see [5] for more details). Neglecting Pomeron loop insertions, $\chi_{h(i)}^{\text{loop}}$ and $\chi_{h(i)}^{\text{loop}(1)}$ reduce to the eikonal $\chi_{h(i)}^{\mathbb{P}} = \chi_{h(i)}^{\mathbb{P}\text{soft}} + \chi_{h(i)}^{\mathbb{P}\text{sh}}$ describing an exchange of a soft or semihard Pomeron between the hadron h represented by its GW state $|i\rangle$ and a multi-Pomeron vertex. Here $\chi_{h(i)}^{\mathbb{P}\text{soft}}(y, b)$ is obtained from Eq. (18), for $s = s_0 e^y$, replacing the vertex factor $\gamma_{p(j)}$ by $\gamma_{\mathbb{P}}$ and $R_{p(j)}^2$ by $R_{3\mathbb{P}}^2 \simeq 0$:

$$\chi_{h(i)}^{\mathbb{P}\text{soft}}(y, b) = \frac{\gamma_{h(i)} \gamma_{\mathbb{P}} e^{(\alpha_{\mathbb{P}}(0)-1)y}}{R_{h(i)}^2 + \alpha'_{\mathbb{P}}(0)y} e^{\frac{-b^2/4}{R_{h(i)}^2 + \alpha'_{\mathbb{P}}(0)y}}. \quad (27)$$

In turn, $\chi_{h(i)}^{\mathbb{P}\text{sh}}(y, b)$ is obtained from Eq. (20), for $s = s_0 e^y$, replacing $\chi_{p(j)}^{\mathbb{P}\text{soft}}$ by $\chi_{J\mathbb{P}}^{\mathbb{P}\text{soft}}$, with

$$\begin{aligned} \chi_{J\mathbb{P}}^{\mathbb{P}\text{soft}}(\hat{s}, b) = & \frac{\gamma_{\mathbb{P}} V_J^{\mathbb{P}}(s_0/\hat{s})(\hat{s}/s_0)^{\alpha_{\mathbb{P}}(0)-1}}{\alpha'_{\mathbb{P}}(0) \ln(\hat{s}/s_0)} \\ & \times \exp\left[-\frac{b^2}{4\alpha'_{\mathbb{P}}(0) \ln(\hat{s}/s_0)}\right], \quad (28) \end{aligned}$$

where $V_J^{\mathbb{P}}$ is defined by Eqs. (8) and (9), for $\beta_{g/h} = \beta_{g/\pi}$.

In contrast to [4,5], where $\gamma_{\mathbb{P}}$ was treated as an adjustable parameter, here we make a specific choice:

$$\gamma_{\mathbb{P}} = r_{3\mathbb{P}}/(\alpha_{\mathbb{P}}(0) - 1). \quad (29)$$

Taking into account the ‘‘renormalization’’ of the soft Pomeron in the ‘‘dense’’ (high s , small b) limit [32], this pushes it into the ‘‘critical’’ regime in such a limit (see [33] for a recent discussion): with the renormalized Pomeron intercept

$$\alpha_{\mathbb{P}}^{(\text{ren})}(0) = \alpha_{\mathbb{P}}(0) - r_{3\mathbb{P}}/\gamma_{\mathbb{P}} = 1. \quad (30)$$

In turn, this leads to a ‘‘saturation’’ of both partial gluon and sea (anti)quark GPDs $G_{I/h(i)}^{\text{scr}}$ and of the corresponding total GPDs,

$$G_{I/h}^{\text{scr}}(x, b, Q_0^2) = \sum_i C_h^{(i)} G_{I/h(i)}^{\text{scr}}(x, b, Q_0^2), \quad (31)$$

at the virtuality scale Q_0^2 , in the low x and small b limit, for any hadron h [34].

Here, taking into account absorptive corrections due to enhanced Pomeron diagrams, $G_{I/h(i)}^{\text{scr}}$ are defined as⁷ [4,22]

$$\begin{aligned} xG_{I/h(i)}^{\text{scr}}(x, b, Q_0^2) &= \chi_{Ih(i)}^{\mathbb{P}\text{soft}}(s_0/x, b) + G \int d^2b' \\ &\times \int_{\xi}^{-\ln x} dy' \left\{ \chi_{I\mathbb{P}}^{\mathbb{P}\text{soft}}(s_0 e^{-y'}/x, |\vec{b} - \vec{b}'|) \right. \\ &\times \left[\chi_{h(i)}^{\text{loop}}(y', b') - \chi_{h(i)}^{\text{loop}(1)}(y', b') \right] \\ &+ \chi_I^{\text{loop}}(-\ln x - y', |\vec{b} - \vec{b}'|) \\ &\left. \times \left[1 - e^{-\chi_{h(i)}^{\text{fan}}(y', b')} - \chi_{h(i)}^{\text{fan}}(y', b') \right] \right\}. \quad (32) \end{aligned}$$

Here $\chi_{h(i)}^{\text{fan}}$ is a solution of the ‘‘fan’’ diagram equation [cf. Eq. (26)]:

$$\begin{aligned} \chi_{h(i)}^{\text{fan}}(y', b') &= \chi_{h(i)}^{\text{loop}}(y', b') + G \int d^2b'' \\ &\times \int_{\xi}^{y'-\xi} dy'' \left[1 - e^{-\chi_{h(i)}^{\text{loop}}(y'-y'', |\vec{b}' - \vec{b}''|)} \right] \\ &\times \left[1 - e^{-\chi_{h(i)}^{\text{fan}}(y'', b'')} - \chi_{h(i)}^{\text{fan}}(y'', b'') \right], \quad (33) \end{aligned}$$

while χ_I^{loop} is defined as

$$\begin{aligned} \chi_I^{\text{loop}}(y', b') &= \chi_{I\mathbb{P}}^{\mathbb{P}\text{soft}}(s_0 e^{y'}, b') + G \int d^2b'' \\ &\times \int_{\xi}^{y'-\xi} dy'' \chi_{I\mathbb{P}}^{\mathbb{P}\text{soft}}(s_0 e^{y'-y''}, |\vec{b}' - \vec{b}''|) \\ &\times \left[1 - e^{-\chi^{\text{loop}}(y'', b'')} - \chi^{\text{loop}(1)}(y'', b'') \right]. \quad (34) \end{aligned}$$

Applying the AGK cutting rules [10], one was able to obtain the complete set of unitarity cuts of elastic scattering diagrams for hadron-hadron collisions, corresponding to the above-discussed resummation scheme, explicitly verifying the s -channel unitarity of the approach, and to derive positive-definite partial cross sections for all the various configurations of final states, including diffractive ones [30,31]. In turn, those allowed one to develop a MC procedure for generating such configurations both for hadron-proton and for hadron-nucleus (nucleus-nucleus) scattering events [5].

As discussed in [4,22], an important feature of the described approach is a consistency with the collinear factorization of pQCD: by virtue of the AGK cancellations [10], the inclusive parton jet production cross section is defined by the usual factorization ansatz:

$$\begin{aligned} \frac{d\sigma_{hp}^{\text{jet}}(s, p_t)}{dp_t^2} &= K \int dx^+ dx^- \sum_{I,J} f_{I/h}^{\text{scr}}(x^+, \mu_{\mathbb{F}}^2) \\ &\times f_{J/p}^{\text{scr}}(x^-, \mu_{\mathbb{F}}^2) \frac{2d\sigma_{IJ}^{2\rightarrow 2}(x^+ x^- s, p_t^2, \mu_{\mathbb{R}})}{dp_t^2}. \quad (35) \end{aligned}$$

Here the PDFs $f_{I/h}^{\text{scr}}$, with the absorptive corrections taken into account, are expressed via the partial GPDs $G_{I/h(i)}^{\text{scr}}$, Eq. (32), evolving the latter from Q_0^2 to $\mu_{\mathbb{F}}^2$:

$$\begin{aligned} f_{I/h}^{\text{scr}}(x, \mu_{\mathbb{F}}^2) &= \sum_i C_h^{(i)} \int d^2b \sum_{I'} \int_x^1 \frac{dz}{z} \\ &\times E_{I'I}^{\text{QCD}}(z, Q_0^2, \mu_{\mathbb{F}}^2) G_{I'/h(i)}^{\text{scr}}(x/z, b, Q_0^2). \quad (36) \end{aligned}$$

VI. DYNAMICAL POWER CORRECTIONS TO HARD SCATTERING

As mentioned in Sec. V, an important feature of the above-discussed approach is the consistency with the collinear factorization of pQCD: the inclusive jet cross section is defined by Eq. (35). However, this creates an unpleasant sensitivity of the model predictions to the choice of the ‘‘infrared’’ cutoff Q_0^2 : since $d\sigma_{hp}^{\text{jet}}(s, p_t)/dp_t^2$ explodes in the small p_t limit. For example, in case of the QGSJET-II model, a reasonable consistency with collider measurements is reached for a rather high value of that cutoff, $Q_0^2 = 3 \text{ GeV}^2$ [5]. On the other hand, one may expect the pQCD approach to remain applicable for parton virtualities as small as $\sim 1 \text{ GeV}^2$. It is thus natural to ask ourselves

⁷In [4,22], a simplified expression for $G_{I/h(i)}^{\text{scr}}$ had been provided, neglecting Pomeron loop contributions.

whether there exists a perturbative mechanism capable of damping the jet production at small p_t .

To address this question, it is useful to remind oneself that the collinear factorization of pQCD is established at the leading twist level [35,36], i.e., neglecting the so-called higher twist (HT) corrections suppressed by powers of the relevant hard scale. One may thus expect that those are such power corrections which should provide the desirable suppression of low p_t jet production.

Unfortunately, it is hardly possible at the present stage to treat HT effects in hadronic collisions in a systematic way, especially, regarding their potential implementation in MC event generators: in particular, since this involves a significant number of unknown multiparton correlators and the corresponding HT contributions are not generally positive definite, excluding thereby a probabilistic interpretation [37–39]. Therefore, we adopt here a phenomenological approach [34,40], concentrating on a particular class of dynamical power corrections to parton scattering processes, corresponding to coherent multiple rescattering of s -channel partons on virtual soft [characterized by small light cone (LC) momentum fractions, $x_g \sim 0$] gluon pairs [41–43]. Such contributions have been shown to provide dominant nuclear size-enhanced power corrections to the low x and low Q^2 behavior of structure functions (SFs) in deep inelastic scattering (DIS) on nuclear targets [41,42] and to the suppression of jet p_t spectra in high energy proton scattering on heavy nuclei, for moderately small p_t [43].

A. Resummed A -enhanced power corrections [41–43]

Regarding HT corrections to nuclear SFs, the dominant A -enhanced contributions, in the small Bjorken x limit, were shown to come from diagrams of the kind depicted in Fig. 4 (left), corresponding to a rescattering of the struck quark on soft, pairwise singlet, virtual gluon pairs [41,42]. The perturbative hard part of the graph is characterized by a specific structure of the s -channel quark propagators: with the gluon fields in a pair being separated by the so-called “contact” term, implying no propagation along the LC coordinate [44]; propagators which separate such gluon pairs from the quark field and from each other are represented, on the other hand, by pole terms corresponding to a propagation over considerable LC distances. It is such a prescription which gives rise to the nuclear enhancement: in the low x limit, the struck quark from one nucleon in the nucleus propagates over large distances $\propto 1/(xp^+)$, p^+ being the LC-plus (LC⁺) momentum of the nucleon, scattering coherently on many correlated soft gluon pairs from other nucleons [41,42]. Upon the full all-order resummation of such contributions (in the LC $A^+ = 0$ gauge), one obtained the HT correction to the nuclear transverse structure function $F_T^{(A)}$ [cf. Eq. (8) in [41]]:

$$\delta_{HT} F_T^{(A)}(x, Q^2) = \sum_q \frac{e_q^2}{2} \sum_{n \geq 1} \frac{1}{n!} \left[\frac{4\pi^2 \alpha_s x}{3Q^2} \right]^n \frac{d^n}{d^n x} T_q^{(n)} \underbrace{gg \dots}_n(x), \quad (37)$$

where e_q is the fractional charge of (anti)quark q and the multiparton correlators $T_{qgg \dots}^{(n)}$ are defined as

$$T_q^{(n)} \underbrace{gg \dots}_n(x) = \int \frac{dy^-}{4\pi} e^{ip^+ xy^-} \langle A | \bar{\psi}(0) \gamma^+ \times \prod_{i=1}^n \left[\int P^+ dy_{g_i}^- \Theta(y_{g_i}^-) \hat{F}^2(y_{g_i}^-) \right] \psi(y^-) | A \rangle, \quad (38)$$

with

$$\hat{F}^2(y_g^-) = \int \frac{d\tilde{y}_g^-}{2\pi p^+} F^{+\alpha}(y_g^-) F_{\alpha}^+(\tilde{y}_g^-) \Theta(y_g^- - \tilde{y}_g^-). \quad (39)$$

Here y^-, y_g^- are LC-minus (LC⁻) coordinates of the fields and F_{α}^+ is the projection of the gluon field tensor on the LC⁺ direction.

Likewise, in case of nucleus-proton scattering, the dominant A -enhanced HT corrections to jet production cross section arise from the diagrams of Fig. 4 (right), corresponding to a rescattering of the nuclear parton (quark or gluon), participating in the hard scattering, on such soft gluon pairs, with the same structure of s -channel propagators along the struck parton line⁸ [43]. Resumming such contributions to all orders, one obtained [43]

$$\delta_{HT} \frac{d\sigma_{pA}^{\text{jet}}(s, p_t)}{dp_t^2} = \int dx^+ dx^- \times \sum_{I,J} f_{J/p}(x^-, \mu_{\bar{F}}^2) \sum_{n \geq 1} \frac{1}{n!} \left[\frac{-C_I \pi^2 \alpha_s x^+}{\hat{t}} \right]^n \times \frac{d^n}{d^n x} \left[T_q^{(n)} \underbrace{gg \dots}_n(x^+) \frac{2d\sigma_{IJ}^{2 \rightarrow 2}}{dp_t^2} \right], \quad (40)$$

with $C_{q(\bar{q})} = C_F = 4/3$, $C_g = C_A = 3$, and $\hat{t} = q^2$ being the momentum transfer squared for parton-parton scattering. In addition to $T_{qgg \dots}^{(n)}$ defined by Eqs. (38) and (39), Eq. (40) involves multigluon correlators $T_{ggg \dots}^{(n)}$:

⁸Alternative configurations of the hard scattering part of the graph contain contact terms leading to a loss of the A enhancement [43].

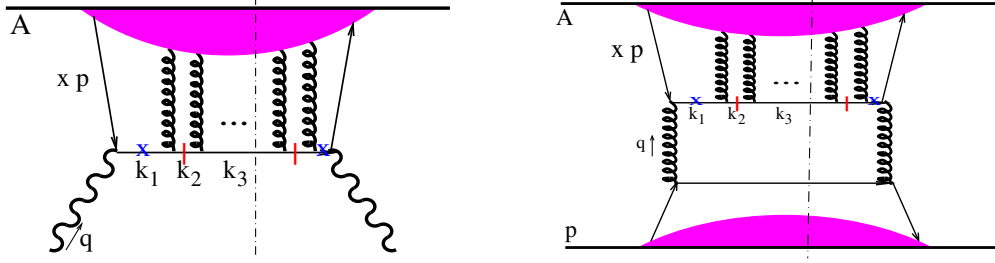


FIG. 4. Example diagrams for dominant A -enhanced power corrections to nuclear DIS (left) and to jet production in proton-nucleus scattering (right). Propagators marked by crosses and vertical dashes correspond to pole and contact terms, respectively.

$$T_{gg\dots}^{(n)}(x) = \int \frac{dy^-}{2\pi x p^+} e^{ip^+ xy^-} \langle A | F^{+\beta}(0) \times \prod_{i=1}^n \left[\int p^+ dy_{g_i}^- \Theta(y_{g_i}^-) \hat{F}^2(y_{g_i}^-) \right] F_{\beta}^+(y^-) | A \rangle. \quad (41)$$

Further, one proposed a model for the multiparton correlators $T_{Igg\dots}^{(n)}$, $I = q, g$: assuming that the dominant contributions to Eqs. (37) and (40) arise from a rescattering of the struck nuclear parton on gluon pairs belonging to different nucleons and performing the corresponding factorization [41]:

$$\langle A | \hat{O}_0 \prod_{i=1}^n \hat{O}_i | A \rangle \propto \langle p | \hat{O}_0 | p \rangle \prod_{i=1}^n \langle p | \hat{O}_i | p \rangle. \quad (42)$$

This allowed one to obtain closed compact results for $F_T^{(A)}$ and $d\sigma_{pA}^{\text{jet}}/dp_t^2$, the power corrections being accounted for:

$$F_T^{(A)}(x, Q^2) \simeq A \sum_q \frac{e_q^2}{2} \times f_{q/p}(x + x C_q \xi^2 (A^{1/3} - 1)/Q^2, Q^2) \quad (43)$$

$$\frac{d\sigma_{pA}^{\text{jet}}(s, p_t)}{dp_t^2} \simeq A \int dx^+ dx^- \times \sum_{I,J} f_{I/p} \left(x^+ - \frac{x^+ C_I \xi^2 (A^{1/3} - 1)}{\hat{t}}, \mu_F^2 \right) \times f_{J/p}(x^-, \mu_F^2) \frac{2d\sigma_{IJ}^{2 \rightarrow 2}}{dp_t^2}, \quad (44)$$

where $\xi^2 \propto \langle p | \hat{F}^2 | p \rangle \propto \lim_{x \rightarrow 0} x f_{g/p}$ defines the characteristic scale of the HT corrections.

B. Phenomenological implementation in QGSJET-III

Since we are going to extrapolate the treatment of [43] to the case of hadron-proton scattering, we need a different approach for modeling the corresponding multiparton

correlators. Starting with the quark-gluon correlator $T_{qg}^{(1)}$, a closer look at Eq. (38) reveals that it formally coincides, up to a factor, with the quark-gluon ^2GPD $F_{qg}^{(2)}$ multiplied by the gluon LC momentum fraction x_g , in the limit $x_g \rightarrow 0$ and for zero transverse separation between the two partons, $\vec{\Delta} = 0$ (see, e.g., [8] for the corresponding definitions), and similarly for $T_{gg}^{(1)}$ in Eq. (41). This motivated us to employ a probabilistic treatment for $T_{qg}^{(1)}$ and $T_{gg}^{(1)}$, interpreting them as $\propto x_g F_{qg}^{(2)}|_{\vec{\Delta}=0}$ and $\propto x_g F_{gg}^{(2)}|_{\vec{\Delta}=0}$, respectively, and to proceed in a similar way with all the other correlators $T_{Igg\dots}^{(n)}$ involving larger numbers of soft gluons.

Here we have to make additional assumptions concerning the relevant virtuality scales and gluon momentum fractions in the corresponding multiparton GPDs, e.g., for Q_q^2, Q_g^2 , and x_g in $F_{qg}^{(2)}(x, x_g, Q_q^2, Q_g^2, \vec{\Delta})$. While the natural choice for Q_q^2 is the factorization scale μ_F^2 for the hard process, one usually considers soft gluons to be purely nonperturbative ones, with $Q_g^2 \sim \Lambda_{\text{QCD}}^2$ (e.g., [45]). Instead, we set Q_g^2 equal to our separation scale Q_0^2 , in order to describe the GPDs by soft Pomeron asymptotics, plus absorptive corrections, Eq. (32).

Finally, assuming a finite virtuality for the soft gluons implies that they have nonzero LC $^{\pm}$ momentum fractions x_g^{\pm} ,

$$|q_g^2| \sim x_g^+ x_g^- s. \quad (45)$$

In the factorization procedure which led to Eqs. (37) and (40), one neglected LC $^-$ momentum components for projectile partons (similarly neglecting LC $^+$ momenta of target partons) and considered the limit $x_g \rightarrow 0$ for the soft gluons involved in the process. Here, taking into account the finite virtuality of such gluons, Eq. (45), and the fact that these gluons belong to the projectile proton (for the case of rescattering on the projectile soft gluons), their LC $^-$ momentum fractions should be much smaller than the LC $^-$ fraction of the target parton participating in the hard process:

$$x_g^- \sim \frac{|q_g^2|}{x_g^+ s} \ll x^-. \quad (46)$$

Since we expect a rather weak x_g dependence for $x_g F_{qg}^{(2)}$ and $x_g F_{gg}^{(2)}$ in the small x_g limit at the low virtuality scale $Q_g^2 = Q_0^2$, we set

$$x_g = \frac{Q_0^2}{x^- s}. \quad (47)$$

Using these additional assumptions, we obtain the leading power correction to the inclusive parton jet production cross section as [cf. Eq. (40)]

$$\begin{aligned} & \delta_{HT}^{(1)} \frac{d\sigma_{hp}^{\text{jet}}(s, p_t)}{dp_t^2} \\ &= K \int dx^+ dx^- \sum_{I,J} f_{J/p}^{\text{scr}}(x^-, \mu_F^2) \\ & \quad \times \frac{K_{\text{HT}} C_I \pi^2 \alpha_s(\mu_R^2) x^+ 2d\sigma_{IJ}^{2 \rightarrow 2}(\hat{s}, p_t^2, \mu_R)}{|\hat{t}| dp_t^2} \\ & \quad \times x_g^+ F_{I/g}^{(2)}(x^+, x_g^+, \mu_F^2, Q_0^2, \vec{\Delta} = \vec{0}) \Big|_{x_g^+ = \frac{Q_0^2}{x^- s}}, \end{aligned} \quad (48)$$

where $\hat{s} = x^+ x^- s$ and, in view of the numerous brute force assumptions made, we introduced an adjustable parameter K_{HT} which controls the magnitude of the HT corrections in our approach.

Including also higher power corrections, accounting for the GW decomposition of hadron wave functions, and expressing multiparton GPDs via single parton ones (thereby neglecting parton-parton correlations at the Q_0^2 scale),

$$\begin{aligned} & F_{I \underbrace{gg \dots}_{n} / h(i)}(x, x_{g_1}, \dots, Q^2, Q_{g_1}^2, \dots, \vec{\Delta}_{g_1}, \dots) \\ & \simeq \int d^2 b_I G_{I/h(i)}^{\text{scr}}(x, b_I, Q^2) \\ & \quad \times \prod_{i=1}^n G_{g/h(i)}^{\text{scr}}(x_{g_i}, |\vec{b}_I + \vec{\Delta}_{g_i}|, Q_{g_i}^2), \end{aligned} \quad (49)$$

considering rescatterings on soft gluon pairs both from the projectile and from the target (taking into account that those become significant in different parts of the kinematic space), we finally get

$$\begin{aligned} \frac{d\sigma_{hp}^{\text{jet}}(s, p_t)}{dp_t^2} & \simeq \int d^2 b \left\{ K \int d^2 b' \sum_{i,j} C_h^{(i)} C_p^{(j)} \right. \\ & \quad \times \int dx^+ dx^- \sum_{I,J} G_{I/h(i)}^{\text{scr}}(x^+ + \tilde{x}^+, b', \mu_F^2) \\ & \quad \left. \times G_{J/p(j)}^{\text{scr}}(x^- + \tilde{x}^-, |\vec{b} - \vec{b}'|, \mu_F^2) \frac{2d\sigma_{IJ}^{2 \rightarrow 2}}{dp_t^2} \right\}, \end{aligned} \quad (50)$$

where

$$\tilde{x}^+ = x^+ \frac{K_{\text{HT}} C_I \pi^2 \alpha_s(\mu_R^2)}{|\hat{t}|} x_g^+ G_{g/h(i)}^{\text{scr}}(x_g^+, b', Q_0^2) \Big|_{x_g^+ = \frac{Q_0^2}{x^- s}} \quad (51)$$

$$\tilde{x}^- = x^- \frac{K_{\text{HT}} C_J \pi^2 \alpha_s(\mu_R^2)}{|\hat{t}|} x_g^- G_{g/p(j)}^{\text{scr}}(x_g^-, |\vec{b} - \vec{b}'|, Q_0^2) \Big|_{x_g^- = \frac{Q_0^2}{x^+ s}}. \quad (52)$$

Like in the original approach of Refs. [41–43], the effect of the considered HT corrections amounts to a shift of the LC^\pm momentum fractions of the active partons I and J , participating in the hard scattering. However, in our case, due to the assumed model for multiparton correlators, the magnitude of these shifts \tilde{x}^\pm , Eqs. (51) and (52), depends on the collision kinematics. Consequently, the overall strength of the HT corrections varies with the energy and impact parameter of the collision, increasing in the dense (high s , small b) limit.

Modifications similar to Eq. (50) apply to all the eikonals describing semihard Pomeron exchanges. For example, $\chi_{hp(ij)}^{\text{Psh}}$, Eq. (20), now takes the form

$$\begin{aligned} \chi_{hp(ij)}^{\text{Psh}}(s, b) &= \frac{K}{2} \sum_{I,J} \int d^2 b' \int dx^+ dx^- \\ & \quad \times \int dp_t^2 G_{I/h(i)}(x^+ + \tilde{x}^+, b', \mu_F^2) \\ & \quad \times G_{J/p(j)}(x^- + \tilde{x}^-, |\vec{b} - \vec{b}'|, \mu_F^2) \\ & \quad \times \frac{d\sigma_{IJ}^{2 \rightarrow 2}(\hat{s}, p_t^2, \mu_R)}{dp_t^2} \Theta(\mu_F - Q_0), \end{aligned} \quad (53)$$

with \tilde{x}^\pm as in Eqs. (51) and (52), and with $G_{I/h(i)}$ being defined neglecting absorptive corrections [cf. Eq. (22)]:

$$\begin{aligned} G_{I/h(i)}(x, b, \mu_F^2) &= \sum_I \int_x^1 dz \\ & \quad \times E_{I'I}^{\text{QCD}}(z, Q_0^2, \mu_F^2) \chi_{Ih(i)}^{\text{Psoft}}(s_0 z/x, b)/x. \end{aligned} \quad (54)$$

Neglecting the HT corrections, i.e., setting $K_{\text{HT}} = 0$, Eqs. (35) and (20) are recovered from Eqs. (50) and (53), respectively.

In turn, for the proton structure function $F_2^{(p)}$ we obtain, using the same assumptions,

$$\begin{aligned} F_2^{(p)}(x, Q^2) & \simeq x \sum_q e_q^2 \int d^2 b \sum_i C_p^{(i)} \\ & \quad \times G_{q/p(i)}^{\text{scr}}(x + \tilde{x}, b, Q^2), \end{aligned} \quad (55)$$

with

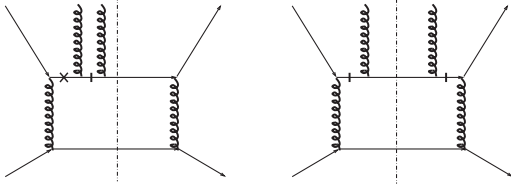


FIG. 5. Left: the structure of the hard “blob” in Fig. 4 (right), for leading power corrections discussed in the text, for the case of hard scattering of quarks of different flavors. Right: an alternative leading power correction to the qq' hard scattering, which provides a subleading contribution in the high energy limit.

$$\tilde{x} = \frac{4K_{\text{HT}}\pi^2\alpha_s(Q^2)x}{3Q^2} x_g G_{g/p(i)}^{\text{scr}}(x_g, b, Q_0^2) \Big|_{x_g = \frac{xQ_0^2}{Q^2}} \quad (56)$$

At this point, we have to provide some arguments to support our extrapolation of the treatment of [43] to the case of hadron-proton scattering. In particular, here we cannot use the A -enhancement argument to neglect other potential HT contributions characterized by a different structure of the hard scattering part, compared to the one in Fig. 5 (left), considered so far. To this end, let us remind ourselves that the Lorentz contraction acts differently on partons of different momenta, in a fast-moving parton cloud of a hadron. While fast (large x) partons are confined to a narrow “pancake” in the longitudinal direction, the abundant small x gluons are spread over longitudinal distances $\propto 1/(xp^+)$. For the diagram in Fig. 5 (left), corresponding to the approach of [43], the struck low- x quark propagates over large distances $\propto 1/(x^+p^+)$ comparable to the longitudinal size of the gluon cloud and, thus, may scatter coherently on many correlated soft gluon pairs. In contrast, considering, for example, an alternative configuration depicted in Fig. 5 (right), the first gluon is separated from the quark by the contact propagator, which implies there is a very small distance between the quark and the gluon in the LC^- direction. Hence, only a very small portion of the gluon content of the proton can be involved in that type of interaction, with the corresponding contribution being a subdominant one.

VII. NUCLEAR COLLISIONS AND MONTE CARLO IMPLEMENTATION

The generalization of the model for the treatment of hadron-nucleus and nucleus-nucleus collisions is performed without introducing any additional adjustable parameters, similarly to the case of the QGSJET-II model [5]. The only additional input is nucleon densities for nuclear ground states, chosen according to the corresponding experimental measurements⁹ [46].

⁹For light nuclei, with mass number $A \leq 10$, Gaussian distributions are used, while densities of heavier nuclei are described by three parameter Wood-Saxon distributions.

As discussed in [5], in case of hA and AA collisions, enhanced Pomeron diagrams account for rescattering of intermediate partons off different nucleons from the projectile or/and from the target, i.e., multi-Pomeron vertices generally couple together sequences of Pomerons and Pomeron loops connected to different nucleons. This gives rise to a dynamical treatment of the corresponding absorptive corrections: the strength of such nonlinear effects increases with the collision energy, with the size of the colliding nuclei, and with the “centrality” of the collision.

The very same tendencies hold also for the HT effects discussed in Sec. VI, for hA and AA collisions. Indeed, the multiparton correlators, Eqs. (38) and (41), involve in those cases soft gluons emitted by different nucleons. Describing such correlators by multiparton GPDs, the HT corrections rise in the low x and small b limits, increasing also with the size of the nuclei.

The MC procedure for generating individual inelastic scattering events is almost identical to the one of the QGSJET-II model [5]: starting from sampling the impact parameter for a collision, according to the respective interaction profile, and proceeding to specifying a “macro-configuration” of the event, i.e., defining the structure of the corresponding cut Pomeron “net,” based on partial cross sections for such macroconfigurations. This is followed by sharing the energy-momentum between all elementary parton cascades (cut Pomerons) and choosing, with the appropriate weight, whether a particular cut Pomeron involves a purely soft ($|q^2| < Q_0^2$) parton evolution or corresponds to a semihard parton cascade. In the latter case, one generates explicitly the initial and final state parton emission, treating the respective t - and s -channel parton cascades, using the DGLAP formalism.

More specifically, the initial (t -channel) parton emission is modeled using a forward evolution algorithm, based on an integral representation of the DGLAP equations. For any parton (sub)ladder of mass squared \hat{s} , with the ladder “leg” partons I and J , characterized by virtualities q_1^2 and q_2^2 , respectively ($q_1^2 = q_2^2 = Q_0^2$ for first partons in a particular perturbative cascade), one considers a successive emission of a parton from any of the ladder “ends,” according to the probability (see, e.g., [16] for more details):

$$\begin{aligned} f_{I'}(z, q^2) &\propto \frac{\alpha_s(q^2)}{2\pi q^2} P_{I'I}(z) \Delta_I^S(q_1^2, q^2) \\ &\times \sigma_{IJ}^{\text{QCD}}(z\hat{s}, q^2, q_2^2) \Theta(1 - \varepsilon - z) \Theta(q^2 - q_1^2) \\ &\times \Theta(z\hat{s}/16 - \max[q^2, q_2^2]), \end{aligned} \quad (57)$$

with I' , z , and q^2 being, respectively, the type, LC (plus or minus) momentum fraction, and virtuality of the new t -channel parton. $P_{I'I}$ are the usual (unregularized) Altarelli-Parisi splitting kernels, σ_{IJ}^{QCD} is the contribution of the remaining subladder, defined by Eq. (6), and $\Delta_I^S(q_1^2, q^2)$ is the so-called Sudakov form factor defining

the probability for no parton emission in the virtuality range $[q_1^2, q^2]$:

$$\Delta_q^S(q_1^2, q^2) = \exp \left[- \int_{q_1^2}^{q^2} \frac{d\tilde{q}^2}{\tilde{q}^2} \int_0^{1-\varepsilon} dz \times \frac{\alpha_s(\tilde{q}^2)}{2\pi} P_{qq}(z) \right] \quad (58)$$

$$\Delta_g^S(q_1^2, q^2) = \exp \left[- \int_{q_1^2}^{q^2} \frac{d\tilde{q}^2}{\tilde{q}^2} \int_\varepsilon^{1-\varepsilon} dz \times \frac{\alpha_s(\tilde{q}^2)}{2\pi} \left[\frac{1}{2} P_{gg}(z) + N_f P_{qg}(z) \right] \right]. \quad (59)$$

Here ε is a small enough technical “resolution” parameter (we use $\varepsilon = 10^{-2}$), $N_f = 3$ is the number of active quark flavors, and the last Θ function in Eq. (57) is to assure that the remaining ladder is massive enough to allow for a parton-parton scattering with $p_t^2/4 > \max[q^2, q_1^2]$ (for our choice of the factorization scale, $\mu_F = p_t/2$).

Here comes an important difference, compared to the corresponding treatment of [5]. The generation of macro-configurations of collisions and the energy-momentum sharing procedure are quite similar to the ones of [5], with the only difference that the respective “general Pomeron” eikonals now contain HT corrections to hard scattering processes, as discussed in Sec. VI. On the other hand, when treating the t -channel parton evolution, a two step procedure is adopted. First, the corresponding parton emission pattern is generated based on the standard DGLAP evolution, as described above, the HT corrections being neglected. Next, the obtained parton configuration is accepted with the probability defined by the ratio of the corresponding partial cross sections taking the HT corrections into account (i.e., accounting for the kinematics-dependent shift of LC^\pm momentum fractions of active partons) or neglecting them. Otherwise, the configuration is rejected and the procedure is repeated. In other words, the HT corrections to the hard scattering pattern are accounted for via a rejection procedure. For brevity, we omit here the corresponding technical details.

In turn, the modeling of the final (s -channel) parton emission follows closely the procedure described in [47], imposing the final transverse momentum cutoff $p_{t,\text{cut}}^2(f) = 0.15$. In particular, one assures angular ordering of sequential s -channel subcascades, resulting from color coherence effects [48,49].

As the final step, one considers a formation of strings of color field, stretched between constituent partons of the interacting hadrons (nuclei) or/and between the final s -channel partons resulting from the above-discussed treatment of perturbative parton cascades, following the directions of the corresponding color flows. The breakup and hadronization of such strings is modeled by means

of a string fragmentation procedure, to be discussed elsewhere [7]. Here two important comments are in order. First, the color connections between final partons are defined based on the $1/N_c$ approximation (N_c being the number of colors): following the directions of the color and “anticolor” flows [50]. For each s -channel gluon emission, there are two alternative ways (taken with equal probabilities) to continue such flows, such that a diagram with n s -channel gluons can produce up to 2^n possible patterns for the string configuration (see [18] for a recent detailed discussion). Second, in the hadronization procedure of the QGSJET-III model, inherited from the original QGSJET [3], one considers a nonperturbative splitting of final gluons into quark-antiquark pairs, with the strings having such (anti)quarks at the ends, without gluon “kink” perturbations. Such an approach is generally inferior in quality, compared to more advanced “kinky string” hadronization procedures [50,51] employed in the PYTHIA [52] and EPOS [53] MC generators, notably, regarding high p_t production of relatively heavy hadrons.

VIII. SELECTED RESULTS AND DISCUSSION

The parameters of the model have been fixed using experimental data on total, elastic, and diffractive hadron-proton cross sections, on the proton SF F_2 , and on secondary hadron production in hp and hA collisions,¹⁰ the corresponding values being compiled in Table I. As one can see in the Table, replacing the projectile proton by pion or kaon, subject to a change are only the parameters describing the transverse sizes of GW Fock states of the hadrons.

In Fig. 6, we compare the calculated energy dependence of the total σ_{pp}^{tot} and elastic σ_{pp}^{el} proton-proton cross sections to accelerator data. Additionally, we show by dashed lines the corresponding results obtained neglecting the HT corrections, i.e., setting $K_{\text{HT}} = 0$, while keeping all the other parameters unchanged. In turn, dotted lines correspond to the case of all nonlinear effects being neglected, i.e., setting also the triple-Pomeron coupling $r_{3\text{P}} = 0$. It is easy to see that the highest impact on the \sqrt{s} dependence of $\sigma_{pp}^{\text{tot/el}}$ is due to absorptive corrections generated by enhanced Pomeron diagrams. On the other hand, the considered HT corrections also affect somewhat the calculated $\sigma_{pp}^{\text{tot/el}}$ at sufficiently high energies.

Even such a moderate effect on $\sigma_{pp}^{\text{tot/el}}$ may seem somewhat surprising since the HT corrections apply to hard scattering processes only. Such processes can be expected to dominate relatively central (small b) collisions of hadrons, while having a weak impact on the large b behavior of the scattering amplitude. In that regard, it is

¹⁰A comparison with experimental data on secondary hadron production and a discussion of model parameters related to the hadronization procedure will be presented elsewhere [7].

TABLE I. Model parameters.

$\alpha_{\mathbb{P}}(0)$	$\alpha'_{\mathbb{P}}(0)$ GeV ⁻²	Q_0^2 GeV ²	$r_{3\mathbb{P}}$ GeV ⁻¹	K_{HT}	$r_{g/\mathbb{P}}$	w_{qg}	ξ	β_p	β_π	g_0	d_p	d_π	d_K	$R_{p(1)}^2$ GeV ⁻²	$R_{\pi(1)}^2$ GeV ⁻²	$R_{K(1)}^2$ GeV ⁻²
1.21	0.21	2	0.3	2.5	0.11	0.28	1.5	4	2	2	0.11	0.2	0.28	5.58	1.9	1.12

useful to remind oneself that in the semihard Pomeron scheme employed here, hard parton scattering is preceded by a long enough “soft preevolution” [16,17], as discussed in Sec. III. With increasing energy, such soft parton evolution covers a larger rapidity interval and the corresponding transverse diffusion gives rise to a substantial widening of the transverse profile for semihard scattering processes. This is illustrated in Fig. 7, where the transverse profile for the absorptive part of the inelastic cross section, $d^2\sigma_{pp}^{\text{abs}}/d^2b$, for pp collisions at $\sqrt{s} = 10^2$, 10^3 , and 10^4 GeV is plotted, together with partial contributions of purely soft (i.e., with only soft Pomerons being cut) or semihard (with some “real” parton cascades entering the perturbative, $|q^2| > Q_0^2$, domain) particle production. Additionally shown by dash-dotted lines is the semihard contribution calculated without the HT corrections, i.e., setting $K_{\text{HT}} = 0$. As it is easy to see in the figure, not only the normalization of the profile for semihard interactions rises with energy but also its width increases, corresponding to such interactions happening at larger and larger impact parameters. Further noteworthy is the strong damping of purely soft production processes at small b and large \sqrt{s} , caused by absorptive corrections due to virtual semihard scattering processes¹¹—see the dotted lines in Fig. 7.

What may also seem surprising are the relatively similar shapes of the semihard scattering profiles calculated with and without the HT corrections: dashed and dash-dotted lines in Fig. 7. Here we remind ourselves that those corrections involve soft gluon GPDs $G_{g/p}(x, b, Q_0^2)$ at small x . Since those GPDs are described by soft Pomeron asymptotics (plus the relevant absorptive corrections), cf. Eqs. (31) and (32), the corresponding significant transverse diffusion gives rise to a rather large slope for these GPDs, in the low x limit, which exceeds the one for the semihard scattering itself. As a consequence, these HT corrections mainly reduce the normalization of the semihard interaction profile, without modifying significantly its shape.

In relation to the model treatment of color fluctuations, it is worth comparing the same profiles as in Fig. 7, for partial contributions of different combinations of GW Fock states $|i\rangle$ and $|j\rangle$ of the projectile and target protons, respectively, as plotted in Fig. 8. The first thing to notice is the quick

energy rise of the relative importance of smaller size GW states: both due to increasing opaqueness of the corresponding profiles at small b and due to a fast transverse broadening of these profiles. The two effects are due to, respectively, the low x rise of the (initially small at large x) parton densities and due to the quick transverse expansion of the (initially compact) parton “clouds” of small size GW states. Second, the damping of purely soft hadron production is substantially stronger for larger size GW states, owing to their larger (integrated) parton densities. Likewise, the HT corrections to the calculated transverse profiles are more significant for larger GW Fock states: because of larger soft gluon densities of those states.

In Fig. 9, we compare the calculated proton SF $F_2^{(p)}$, Eq. (55), to the corresponding HERA data, plotting also the results obtained either by suppressing the corresponding HT corrections (setting $K_{\text{HT}} = 0$) or by neglecting all nonlinear effects (setting also $r_{3\mathbb{P}} = 0$). As one can see in the figure, the considered power corrections have a significant impact on the calculated proton SF F_2 at relatively small values of Q^2 , with the effect vanishing for sufficiently high Q^2 . Clearly, these data constrain considerably the magnitude of the HT corrections in the model, i.e., the value of the parameter K_{HT} . On the other hand, a much more serious effect is due to the taming of the low x rise of proton PDFs, caused by absorptive corrections

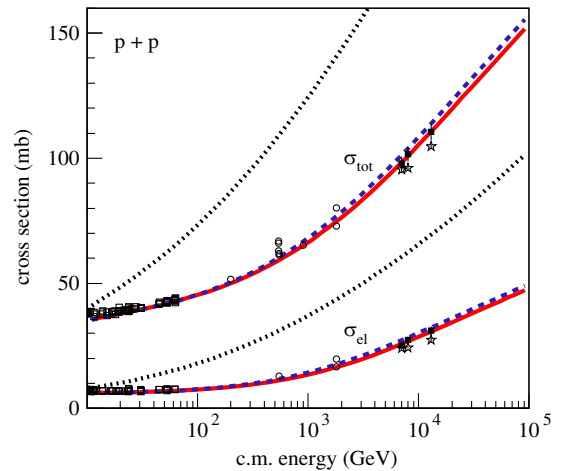


FIG. 6. Calculated energy dependence of the total and elastic pp cross sections—solid lines. The results obtained omitting the HT corrections or neglecting all nonlinear effects are shown by dashed and dotted lines, respectively. The experimental data (points) are from Refs. [54,55].

¹¹Roughly speaking, the corresponding damping factor can be interpreted as the probability to have no semihard production at the respective b values.

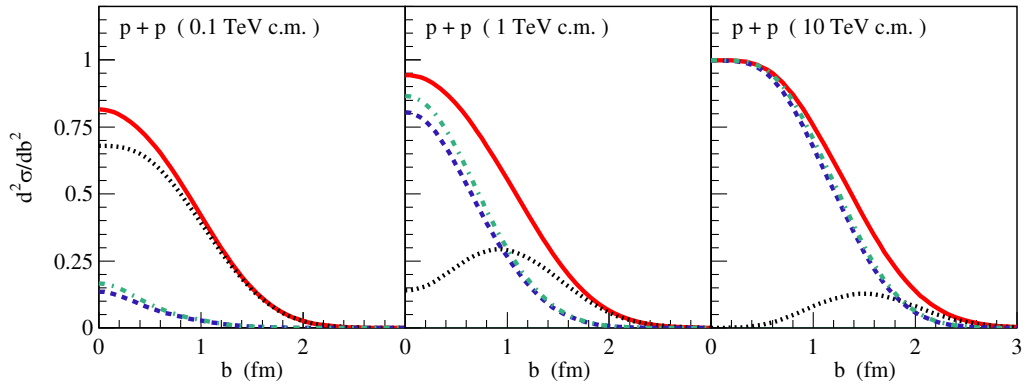


FIG. 7. Calculated transverse profile for the absorptive part of $\sigma_{pp}^{\text{inel}}$ for $\sqrt{s} = 10^2$ (left), 10^3 (middle), and 10^4 GeV (right)—solid lines. Partial contributions of soft and semihard production processes are shown by dotted and dashed lines, respectively. Dash-dotted lines correspond to the latter contribution calculated neglecting the HT corrections.

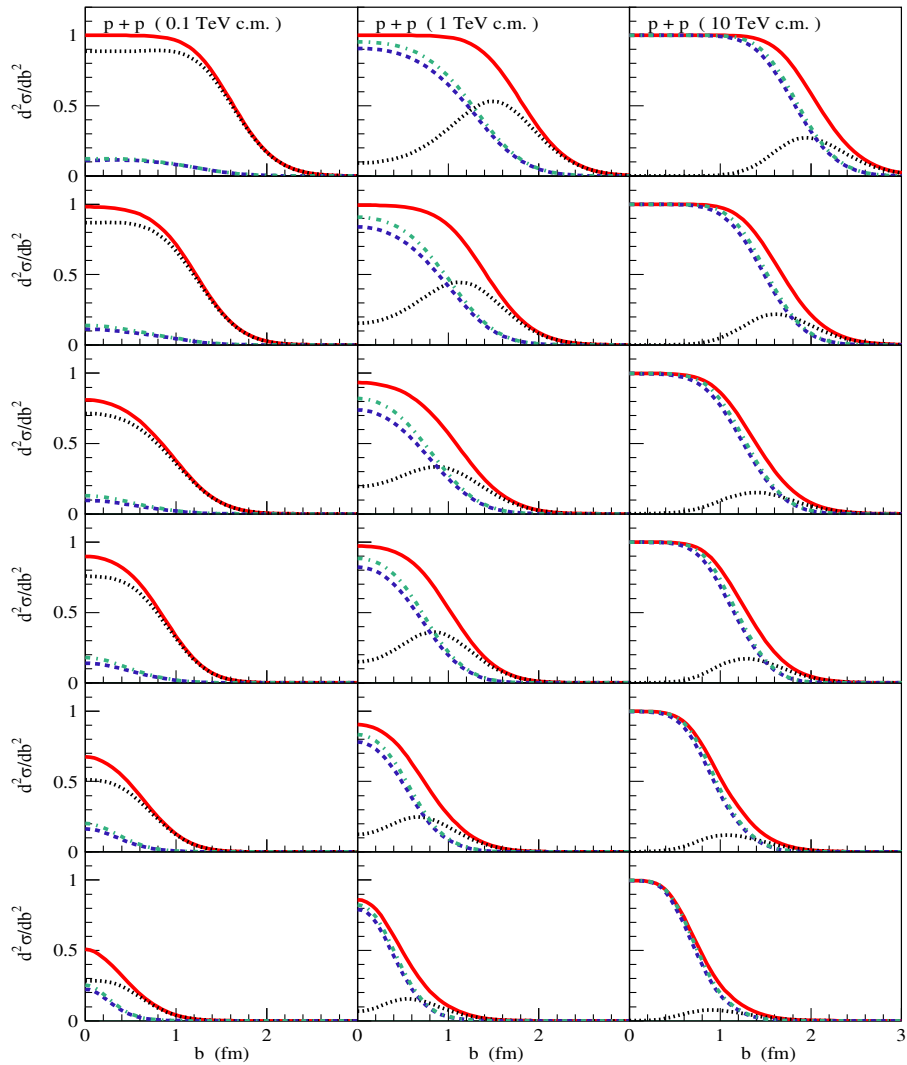


FIG. 8. Same as in Fig. 7, for particular combinations of GW states $|i\rangle$ and $|j\rangle$ of the projectile and target protons, from top to bottom: $(i, j) = (1, 1), (1, 2), (1, 3), (2, 2), (2, 3), (3, 3)$.

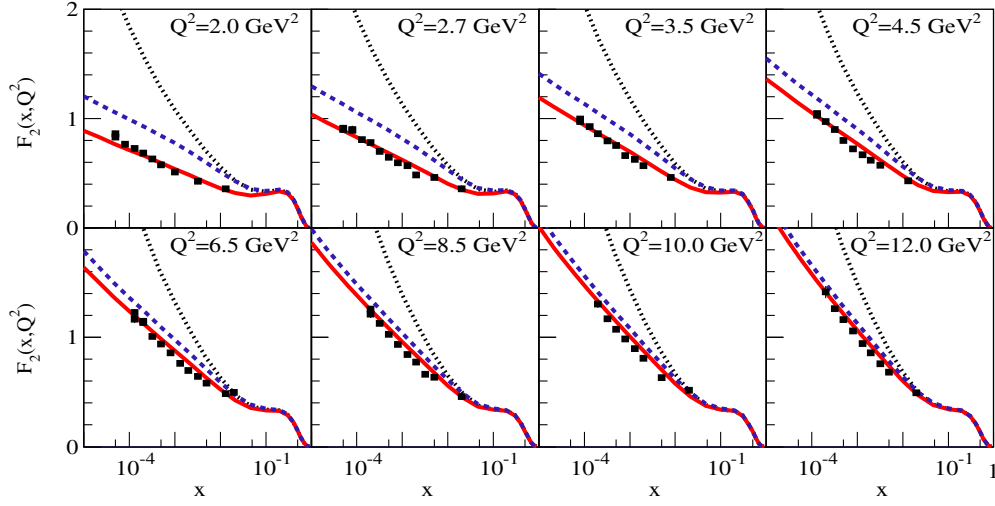


FIG. 9. Calculated x dependence of the proton structure function $F_2^{(p)}(x, Q^2)$, for different Q^2 , as indicated in the plots, compared to HERA data [57].

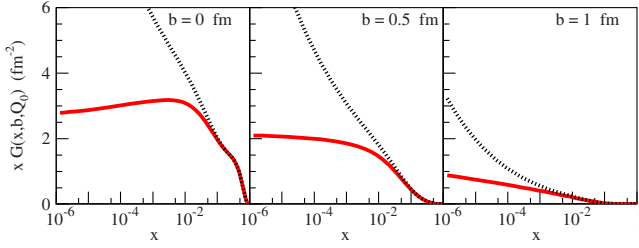


FIG. 10. Gluon GPD $xG_{g/p}(x, b, Q_0^2)$ for different values of b (as indicated in the plots), calculated with (solid lines) and without (dotted lines) absorptive corrections due to Pomeron-Pomeron interactions.

due to enhanced Pomeron graphs. To discuss the latter in more detail, it is worth considering the x dependence of the gluon GPD $G_{g/p}(x, b, Q_0^2)$, calculated with and without such corrections, for different b values [34,56], as plotted in Fig. 10. Here one clearly sees the strong b dependence of nonlinear effects due to Pomeron-Pomeron interactions: while being moderate at large b , such corrections damp strongly the low x rise of the gluon GPD in the $b \rightarrow 0$ limit, causing a saturation of the gluon density.

It is worth considering also the same dependence for partial gluon GPDs of different GW Fock states, $G_{g/p(i)}(x, b, Q_0^2)$, as plotted in Fig. 11. Here we observe the strongest impact of nonlinear effects on the low x behavior of the partial GPDs of the largest Fock states: as a consequence of their largest soft parton densities.

In Fig. 12, we compare the calculated differential elastic cross section $d\sigma_{pp}^{\text{el}}/dt$ to experimental measurements. While the agreement with the data is satisfactory for small values of $|t|$, where the bulk of the contribution to σ_{pp}^{el} comes from, this is not the case for larger $|t| \gtrsim 0.2$. Generally, a better description of the observed t dependence

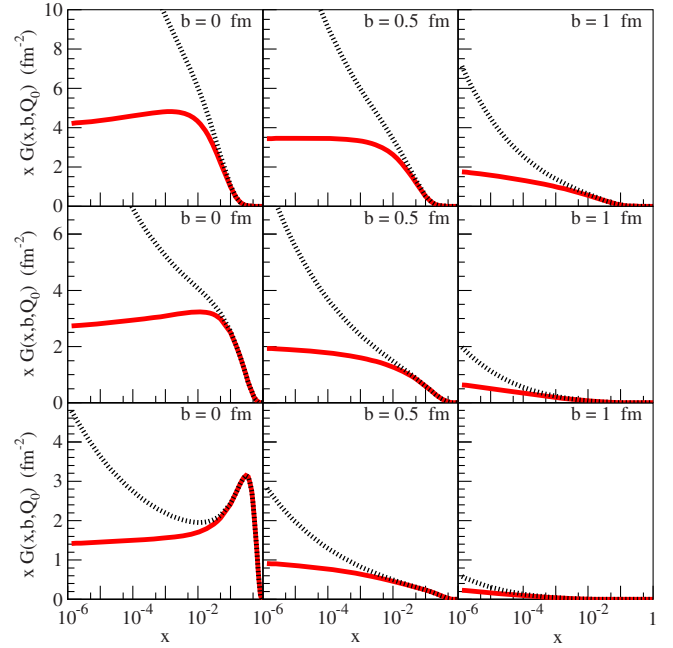


FIG. 11. Same as in Fig. 10, for partial gluon GPDs, $xG_{g/p(i)}(x, b, Q_0^2)$, of different GW Fock states; from top to bottom: $i = 1, 2, 3$.

of $d\sigma_{pp}^{\text{el}}/dt$ requires a more sophisticated choice for the proton form factor (see, e.g., [58]), compared to the simple Gaussian ansatz used in the current work. Moreover, for relatively large $|t|$, the simple GW decomposition of the proton wave function, with t -independent partial weights and profiles of GW Fock states, becomes invalid [59]. Since the presented model aims at describing the bulk of general hadronic and nuclear scattering processes, such potential developments are beyond the scope of the current study.

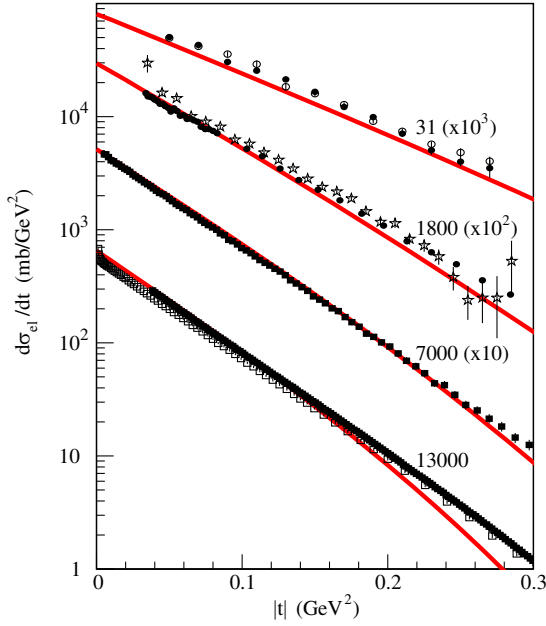


FIG. 12. Calculated differential elastic proton-proton cross section for different \sqrt{s} in GeV (as indicated in the plot), compared to experimental data (points) from Refs. [55,60–64].

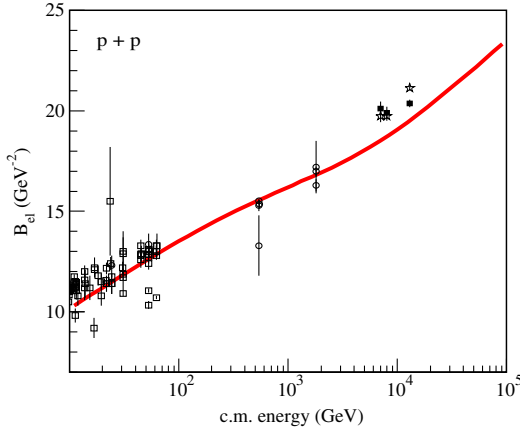


FIG. 13. Energy dependence of the calculated forward elastic scattering slope for pp collisions, compared to experimental data (points) from Refs. [54,55,63,64,67–69].

Additionally, in Fig. 13, we compare to experimental data the calculated \sqrt{s} dependence of the elastic scattering slope $B_{pp}^{\text{el}} = d \ln d\sigma_{pp}^{\text{el}}/dt|_{t=0}$, which quantifies the energy dependence of the average squared impact parameter $\langle b^2 \rangle$ for pp collisions. Clearly, the model fails to reproduce the rather large values of B_{pp}^{el} , reported by the TOTEM and ATLAS collaborations at LHC energies. On the one side, this may be related to additional physics mechanisms missing in the model, like the pion loop contributions to the Pomeron Regge trajectory [65] (see [66] for a recent discussion). On the other hand, it may indicate a certain deficiency of the treatment of color fluctuations in the

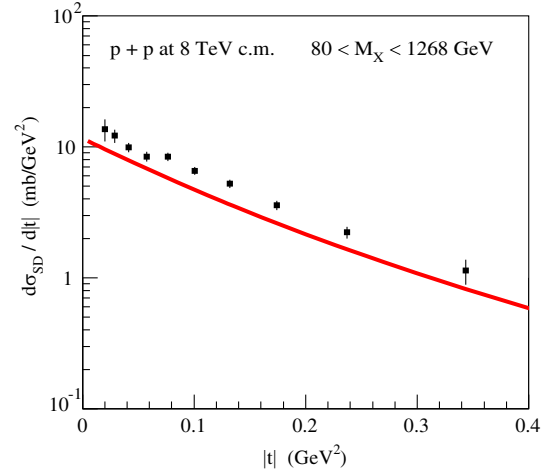


FIG. 14. Calculated $d\sigma_{pp}^{\text{SD}}/dt$ at $\sqrt{s} = 8$ TeV, for $10^{-4} < \xi < 10^{-1.6}$, compared to ATLAS data (points) [72].

model: as one can see in Fig. 13, the increasing relative importance of smaller size GW states slows down the energy rise of B_{pp}^{el} at $\sqrt{s} \gtrsim 1$ TeV.

Let us now come to the model predictions for the inelastic diffraction. In view of a certain tension between different LHC results on the cross section for high mass diffraction, discussed previously in [70,71], of significant importance is the recent measurement by the ATLAS experiment of the differential single diffractive (SD) cross section, $d\sigma_{pp}^{\text{SD}}/dt$, at $\sqrt{s} = 8$ TeV, using the Roman Pot technique [72]. Comparing in Fig. 14 the calculated¹² $d\sigma_{pp}^{\text{SD}}/dt$, for the experimental event selection $10^{-4} < \xi = M_X^2/s < 10^{-1.6}$, M_X being the diffractive state mass, with the ATLAS data, we observe a rather good agreement for the obtained t dependence, while the magnitude of the calculated cross section (1.4 mb) is $\sim 25\%$ below the measured value, 1.88 ± 0.15 mb.¹³

Finally, to illustrate the impact of the considered HT effects on secondary hadron production, we compare in Fig. 15 the p_t dependence of the (mini)jet production cross section, $d\sigma_{pp}^{\text{jet}}(s, p_t)/dp_t^2$, at $\sqrt{s} = 10^2, 10^3$, and 10^4 GeV, as calculated with and without the HT corrections, i.e., using Eqs. (50) and (35), respectively. It is easy to see that such corrections reduce $d\sigma_{pp}^{\text{jet}}(s, p_t)/dp_t^2$ considerably in the small p_t limit, with the suppression becoming more and more significant at higher energies. On the other hand, as expected, the effect vanishes for sufficiently high p_t . Additionally, in Fig. 16, we consider contributions of

¹²The calculation involves a Fourier transform to impact parameter space, in order to account for all the relevant absorptive corrections (see, e.g., [73]).

¹³Taking into account that an additional $\sim 40\%$ contribution to the measured cross section, for the selected ξ -range, comes from nondiffractive production [7] (so-called random rapidity gaps [74]), the total SD-like event rate predicted actually exceeds the measurement by $\sim 20\%$.

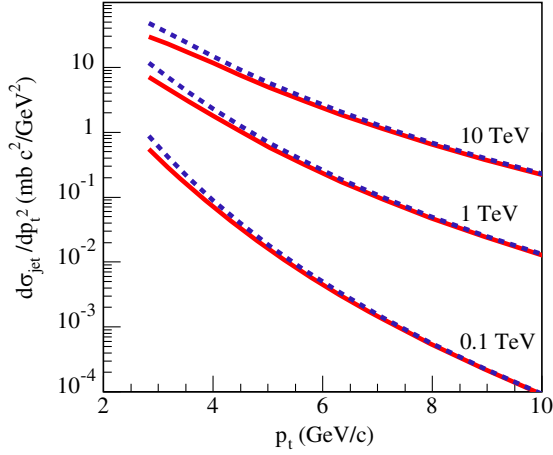


FIG. 15. Transverse momentum spectrum for (mini)jet production in pp collisions at $\sqrt{s} = 10^2, 10^3, \text{ and } 10^4$ GeV, as indicated in the plot, calculated with and without HT corrections—solid and dashed lines, respectively.

different impact parameters to these jet spectra, i.e., we plot $d^3\sigma_{pp}^{\text{jet}}(s, p_t)/dp_t^2/d^2b$ defined by the expression in the curly brackets in Eq. (50). The impact of the considered HT corrections on low p_t (mini)jet production becomes maximal for $b \simeq 0$, while decreasing slowly with the increase of b .

IX. CONCLUSIONS

We presented here a new model for high energy hadronic scattering, QGSJET-III, discussing in some detail its underlying theoretical mechanisms. In particular, considerable attention has been devoted to a phenomenological treatment of dynamical power corrections to hard parton scattering processes, based on the approach of Refs. [41,43]: with the respective contributions being related to coherent rescattering of s -channel partons on soft gluon pairs emitted by the colliding hadrons (nuclei). Modeling the corresponding multiparton correlators as multiparton GPDs, we developed a dynamical scheme: with the strength of the HT effects increasing both in the very high energy and small impact parameter limits.

Additionally, we discussed in some detail the model implementation of color fluctuation effects: based on a decomposition of hadron wave functions in a number of GW Fock states characterized by different transverse sizes and different parton densities.

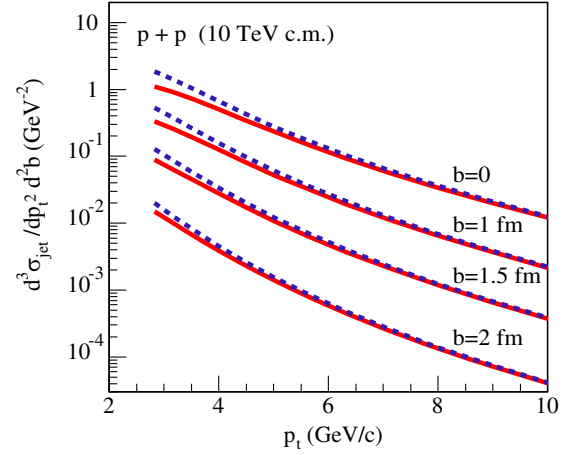


FIG. 16. Transverse momentum spectrum for (mini)jet production in pp collisions at $\sqrt{s} = 10^4$ GeV, for different impact parameters, as indicated in the plot, calculated with and without HT corrections—solid and dashed lines, respectively.

Selected model results regarding the energy dependence of the total and elastic proton-proton cross sections, the x dependence of the proton SF F_2 , the x and b dependence of the gluon GPD $G_{g/p}(x, b, Q_0^2)$, and the t dependence of single-diffractive pp cross section have been presented and the impact of various nonlinear corrections to the interaction dynamics has been investigated. Overall, the most important feature of the model is the microscopic treatment of nonlinear effects due to Pomeron-Pomeron interactions, which is inherited from the previous model version, QGSJET-II. On the other hand, the developed phenomenological treatment of HT effects serves the principal goal: taming the steep rise of the (mini)jet production in the small p_t limit, thereby reducing considerably the sensitivity of the model results to the choice of the infrared cutoff Q_0^2 , as discussed previously in [34].

The description of secondary hadron production and applications of the model to modeling the development of CR-induced extensive air showers will be discussed elsewhere [7].

ACKNOWLEDGMENTS

This work was supported by Deutsche Forschungsgemeinschaft (Project No. 465275045).

- [1] N. N. Kalmykov and S. S. Ostapchenko, The nucleus-nucleus interaction, nuclear fragmentation, and fluctuations of extensive air showers, *Phys. At. Nucl.* **56**, 346 (1993).
- [2] N. N. Kalmykov, S. S. Ostapchenko, and A. I. Pavlov, EAS and a quark-gluon string model with jets, *Bull. Russ. Acad. Sci. Phys.* **58**, 1966 (1994).
- [3] N. N. Kalmykov, S. S. Ostapchenko, and A. I. Pavlov, Quark-gluon string model and EAS simulation problems at ultra-high energies, *Nucl. Phys. B, Proc. Suppl.* **52B**, 17 (1997).
- [4] S. Ostapchenko, Nonlinear screening effects in high energy hadronic interactions, *Phys. Rev. D* **74**, 014026 (2006).
- [5] S. Ostapchenko, Monte Carlo treatment of hadronic interactions in enhanced Pomeron scheme: QGSJET-II model, *Phys. Rev. D* **83**, 014018 (2011).
- [6] S. Ostapchenko, QGSJET-II: Physics, recent improvements, and results for air showers, *EPJ Web Conf.* **52**, 02001 (2013).
- [7] S. Ostapchenko, QGSJET-III model of high energy hadronic interactions: II. Particle production and extensive air shower characteristics (to be published).
- [8] M. Diehl, D. Ostermeier, and A. Schafer, Elements of a theory for multiparton interactions in QCD, *J. High Energy Phys.* **03** (2012) 089.
- [9] V. N. Gribov, A Reggeon diagram technique, *Sov. Phys. JETP* **26**, 414 (1968).
- [10] V. A. Abramovsky, V. N. Gribov, and O. V. Kancheli, Character of inclusive spectra and fluctuations produced in inelastic processes by multi-Pomeron exchange, *Sov. J. Nucl. Phys.* **18**, 308 (1974).
- [11] A. B. Kaidalov and K. A. Ter-Martirosyan, Pomeron as quark-gluon strings and multiple hadron production at SPS collider energies, *Phys. Lett.* **117B**, 247 (1982).
- [12] A. Capella, U. Sukhatme, C.-I. Tan, and J. Tran Thanh Van, Dual parton model, *Phys. Rep.* **236**, 225 (1994).
- [13] A. B. Kaidalov, Quark and diquark fragmentation functions in the model of quark gluon strings, *Sov. J. Nucl. Phys.* **45**, 902 (1987).
- [14] L. Gribov, E. Levin, and M. Ryskin, Semihard processes in QCD, *Phys. Rep.* **100**, 1 (1983).
- [15] H. J. Drescher, M. Hladik, S. Ostapchenko, and K. Werner, A unified treatment of high-energy interactions, *J. Phys. G* **25**, L91 (1999).
- [16] H. J. Drescher, M. Hladik, S. Ostapchenko, T. Pierog, and K. Werner, Parton based Gribov-Regge theory, *Phys. Rep.* **350**, 93 (2001).
- [17] S. Ostapchenko, H. J. Drescher, F. M. Liu, T. Pierog, and K. Werner, Consistent treatment of soft and hard processes in hadronic interactions, *J. Phys. G* **28**, 2597 (2002).
- [18] K. Werner and B. Guiot, Perturbative QCD concerning light and heavy flavor in the EPOS4 framework, *Phys. Rev. C* **108**, 034904 (2023).
- [19] V. N. Gribov and L. N. Lipatov, Deep inelastic e p scattering in perturbation theory, *Sov. J. Nucl. Phys.* **15**, 438 (1972).
- [20] G. Altarelli and G. Parisi, Asymptotic freedom in parton language, *Nucl. Phys.* **B126**, 298 (1977).
- [21] Yu. L. Dokshitzer, Calculation of the structure functions for deep inelastic scattering and e + e- annihilation by perturbation theory in quantum chromodynamics, *Sov. Phys. JETP* **46**, 641 (1977).
- [22] S. Ostapchenko and M. Bleicher, Double parton scattering: Impact of nonperturbative parton correlations, *Phys. Rev. D* **93**, 034015 (2016).
- [23] E. Levin and C.-I. Tan, Heterotic Pomeron: A unified treatment of high-energy hadronic collisions in QCD, [arXiv:hep-ph/9302308](https://arxiv.org/abs/hep-ph/9302308).
- [24] S. Bondarenko, E. Levin, and C.-I. Tan, High energy amplitude as an admixture of “soft” and “hard” Pomerons, *Nucl. Phys.* **A732**, 73 (2004).
- [25] V. N. Gribov, Glauber corrections and the interaction between high-energy hadrons and nuclei, *Sov. Phys. JETP* **29**, 483 (1969).
- [26] M. L. Good and W. D. Walker, Diffraction dissociation of beam particles, *Phys. Rev.* **120**, 1857 (1960).
- [27] V. A. Khoze, A. D. Martin, and M. G. Ryskin, Dynamics of diffractive dissociation, *Eur. Phys. J. C* **81**, 175 (2021).
- [28] L. Frankfurt, M. Strikman, D. Treleani, and C. Weiss, Evidence for color fluctuations in the nucleon in high-energy scattering, *Phys. Rev. Lett.* **101**, 202003 (2008).
- [29] S. Ostapchenko, On the re-summation of enhanced Pomeron diagrams, *Phys. Lett. B* **636**, 40 (2006).
- [30] S. Ostapchenko, Enhanced Pomeron diagrams: Resummation of unitarity cuts, *Phys. Rev. D* **77**, 034009 (2008).
- [31] S. Ostapchenko, Total and diffractive cross sections in enhanced Pomeron scheme, *Phys. Rev. D* **81**, 114028 (2010).
- [32] A. B. Kaidalov, L. A. Ponomarev, and K. A. Ter-Martirosyan, Total cross-sections and diffractive scattering in a theory of interacting Pomerons with $\alpha_p(0) > 1$, *Sov. J. Nucl. Phys.* **44**, 468 (1986).
- [33] M. G. Ryskin, A. D. Martin, and V. A. Khoze, High-energy strong interactions: From “hard” to “soft,” *Eur. Phys. J. C* **71**, 1617 (2011).
- [34] S. Ostapchenko and M. Bleicher, Taming the energy rise of the total proton-proton cross-section, *Universe* **5**, 106 (2019).
- [35] J. C. Collins, D. E. Soper, and G. F. Sterman, Soft gluons and factorization, *Nucl. Phys.* **B308**, 833 (1988).
- [36] J. C. Collins, D. E. Soper, and G. F. Sterman, Factorization of hard processes in QCD, *Adv. Ser. Dir. High Energy Phys.* **5**, 1 (1989).
- [37] R. L. Jaffe and M. Soldate, Twist four in the QCD analysis of lepton production, *Phys. Lett.* **105B**, 467 (1981).
- [38] R. K. Ellis, W. Furmanski, and R. Petronzio, Power corrections to the parton model in QCD, *Nucl. Phys.* **B207**, 1 (1982).
- [39] R. K. Ellis, W. Furmanski, and R. Petronzio, Unraveling higher twists, *Nucl. Phys.* **B212**, 29 (1983).
- [40] S. Ostapchenko, QGSJET-III model: Physics and preliminary results, *EPJ Web Conf.* **208**, 11001 (2019).
- [41] J.-W. Qiu and I. Vitev, Resummed QCD power corrections to nuclear shadowing, *Phys. Rev. Lett.* **93**, 262301 (2004).
- [42] J.-W. Qiu and I. Vitev, Nuclear shadowing in neutrino nucleus deeply inelastic scattering, *Phys. Lett. B* **587**, 52 (2004).
- [43] J.-W. Qiu and I. Vitev, Coherent QCD multiple scattering in proton-nucleus collisions, *Phys. Lett. B* **632**, 507 (2006).
- [44] J.-W. Qiu, Twist four contributions to the parton structure functions, *Phys. Rev. D* **42**, 30 (1990).

- [45] J. Raufeisen, Relating different approaches to nuclear broadening, *Phys. Lett. B* **557**, 184 (2003).
- [46] H. De Vries, C. W. De Jager, and C. De Vries, Nuclear charge-density-distribution parameters from elastic electron scattering, *At. Data Nucl. Data Tables* **36**, 495 (1987).
- [47] G. Marchesini and B. R. Webber, Simulation of QCD jets including soft gluon interference, *Nucl. Phys.* **B238**, 1 (1984).
- [48] Yu. L. Dokshitzer, D. Diakonov, and S. I. Troian, Hard processes in quantum chromodynamics, *Phys. Rep.* **58**, 269 (1980).
- [49] A. Bassetto, M. Ciafaloni, and G. Marchesini, Jet structure and infrared sensitive quantities in perturbative QCD, *Phys. Rep.* **100**, 201 (1983).
- [50] B. Andersson, G. Gustafson, G. Ingelman, and T. Sjostrand, Parton fragmentation and string dynamics, *Phys. Rep.* **97**, 31 (1983).
- [51] H. J. Drescher, F. M. Liu, S. Ostapchenko, T. Pierog, and K. Werner, Initial condition for QGP evolution from NEXUS, *Phys. Rev. C* **65**, 054902 (2002).
- [52] T. Sjostrand, S. Mrenna, and P. Z. Skands, PYTHIA6.4 physics and manual, *J. High Energy Phys.* **05** (2006) 026.
- [53] K. Werner, F.-M. Liu, and T. Pierog, Parton ladder splitting and the rapidity dependence of transverse momentum spectra in deuteron-gold collisions at RHIC, *Phys. Rev. C* **74**, 044902 (2006).
- [54] R. L. Workman *et al.* (Particle Data Group), Review of particle physics, *Prog. Theor. Exp. Phys.* **2022**, 083C01 (2022).
- [55] G. Aad *et al.* (ATLAS Collaboration), Measurement of the total cross section and ρ -parameter from elastic scattering in pp collisions at $\sqrt{s} = 13$ TeV with the ATLAS detector, *Eur. Phys. J. C* **83**, 441 (2023).
- [56] S. Ostapchenko, Non-linear effects in high energy hadronic interactions, [arXiv:hep-ph/0501093](https://arxiv.org/abs/hep-ph/0501093).
- [57] F. D. Aaron *et al.* (H1 and ZEUS Collaborations), Combined measurement and QCD analysis of the inclusive $e^\pm p$ scattering cross sections at HERA, *J. High Energy Phys.* **01** (2010) 109.
- [58] V. A. Khoze, A. D. Martin, and M. G. Ryskin, Elastic and diffractive scattering at the LHC, *Phys. Lett. B* **784**, 192 (2018).
- [59] L. Frankfurt, V. Guzey, A. Stasto, and M. Strikman, Selected topics in diffraction with protons and nuclei: Past, present, and future, *Rep. Prog. Phys.* **85**, 126301 (2022).
- [60] A. Breakstone *et al.*, A measurement of $\bar{p}p$ and pp elastic scattering at ISR energies, *Nucl. Phys.* **B248**, 253 (1984).
- [61] N. A. Amos *et al.* (E710 Collaboration), $\bar{p}p$ elastic scattering at $\sqrt{s} = 1.8$ TeV from $|t| = 0.034$ GeV/ c^2 to 0.65 GeV/ c^2 , *Phys. Lett. B* **247**, 127 (1990).
- [62] F. Abe *et al.* (CDF Collaboration), Measurement of small angle $\bar{p}p$ elastic scattering at $\sqrt{s} = 546$ GeV and 1800 GeV, *Phys. Rev. D* **50**, 5518 (1994).
- [63] G. Antchev *et al.* (TOTEM Collaboration), Measurement of proton-proton elastic scattering and total cross-section at $\sqrt{s} = 7$ TeV, *Europhys. Lett.* **101**, 21002 (2013).
- [64] G. Antchev *et al.* (TOTEM Collaboration), Elastic differential cross-section measurement at $\sqrt{s} = 13$ TeV by TOTEM, *Eur. Phys. J. C* **79**, 861 (2019).
- [65] A. A. Anselm and V. N. Gribov, Zero pion mass limit in interactions at very high-energies, *Phys. Lett.* **40B**, 487 (1972).
- [66] V. A. Khoze, A. D. Martin, and M. G. Ryskin, t -dependence of the slope of the high energy elastic pp cross section, *J. Phys. G* **42**, 025003 (2015).
- [67] G. Antchev *et al.* (TOTEM Collaboration), Luminosity-independent measurement of the proton-proton total cross section at $\sqrt{s} = 8$ TeV, *Phys. Rev. Lett.* **111**, 012001 (2013).
- [68] G. Aad *et al.* (ATLAS Collaboration), Measurement of the total cross section from elastic scattering in pp collisions at $\sqrt{s} = 7$ TeV with the ATLAS detector, *Nucl. Phys.* **B889**, 486 (2014).
- [69] M. Aaboud *et al.* (ATLAS Collaboration), Measurement of the total cross section from elastic scattering in pp collisions at $\sqrt{s} = 8$ TeV with the ATLAS detector, *Phys. Lett. B* **761**, 158 (2016).
- [70] S. Ostapchenko, LHC data on inelastic diffraction and uncertainties in the predictions for longitudinal extensive air shower development, *Phys. Rev. D* **89**, 074009 (2014).
- [71] V. A. Khoze, A. D. Martin, and M. G. Ryskin, High energy elastic and diffractive cross sections, *Eur. Phys. J. C* **74**, 2756 (2014).
- [72] G. Aad *et al.* (ATLAS Collaboration), Measurement of differential cross sections for single diffractive dissociation in $\sqrt{s} = 8$ TeV pp collisions using the ATLAS ALFA spectrometer, *J. High Energy Phys.* **02** (2020) 042.
- [73] E. G. S. Luna, V. A. Khoze, A. D. Martin, and M. G. Ryskin, Diffractive dissociation re-visited for predictions at the LHC, *Eur. Phys. J. C* **59**, 1 (2009).
- [74] V. A. Khoze, F. Krauss, A. D. Martin, M. G. Ryskin, and K. C. Zapp, Diffraction and correlations at the LHC: Definitions and observables, *Eur. Phys. J. C* **69**, 85 (2010).